JPL PUBLICATION 79-17

Accuracy Aspects of Stereo Side-Looking Radar

F. W. Leberl

March 1, 1979

National Aeronautics and
Space Administration

Jet Propulsion Laboratory
California Institute of Technology
Pasadena, California

The research described in this publication was carried out by the Jet Propulsion Laboratory, California Institute of Technology, under NASA Contract No. NAS7-100.

PREFACE

The work described in this report has partly been carried out at the Radar Science and Applications Group of the Radar Science and Engineering Section, Jet Propulsion Laboratory, while the author was on leave from the Institute of National Surveying and Photogrammetry of the Technical University in Graz, Austria.

Many thanks are due to Dr. C. Elachi and Mr. W. Brown Jr. for the support that the author received during his association with JPL.

ABSTRACT

A study has been performed on accuracy aspects of stereo side-looking radar. The geometry of the radar stereo model and factors affecting visual radar stereo perception are reviewed. This is then employed to define limits to the vertical exaggeration factor of stereo radar and to compare it to that of camera photography.

Radar stereo model accuracies are analyzed with respect to coordinate errors caused by errors of radar sensor position and of range, and with respect to errors of coordinate differences, i.e., cross-track distances and height differences.

CONTENTS

Figures

Tables

SECTION 1

INTRODUCTION

Stereo viewing of side-looking radar images can enhance the interpretation of the images by improved observation of morphological details (Koopmans, 1973), it can be used to measure slopes and relative height differences (Dalke and McCoy, 1968), and it can improve the accuracies of cartographic mapping and point positioning (Gracie, et al., 1970; DBA-Systems, 1974; Leberl, 1978).

Generally the term *stereo* refers to visual perception when an observer views an overlapping stereo image pair and in his brain forms a three-dimensional replica of the imaged area. *Stereo* may also be used for a computation process employing monocular measurements in overlapping images: this may occur with data that generally do not permit visual stereo but may show homologue details in overlapping images that can be identified monocularly.

Radar stereo is perceived like its photographic equivalent, although geometries are quite different (Figure 1). The advent of aircraft side-looking radar (SLR), more recently of satellite radar, e.g., in the Apollo-17 and Seasat missions, and several proposed satellite radar projects such as the Space Shuttle SIR-A, SIR-B, Venus Orbital Imaging Radar (VOIR), have led to a requirement to understand stereo radar.

This report presents some basic considerations on stereo radar, addressing its visual perception and a geometric analysis of its possibilities and limitations. Essentially those aspects will be treated that are valid with synthetic aperture radar, since this is being used on spacecraft.

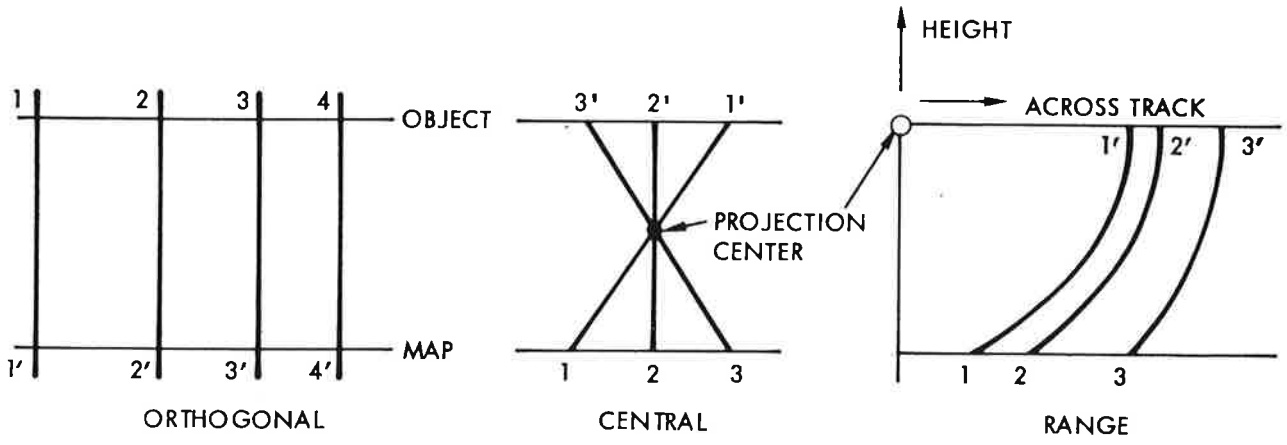

Figure 1. Comparison of Basic Geometries for Orthogonal, Central and Range Projection

SECTION 2
VISUAL RADAR STEREO

2.1 BINOCULAR VISION AND STEREOSCOPIC VIEWING

Visual stereo perception has been analyzed by Aschenbrenner (1952), Fichter (1954), LaPrade (1972, 1973), LaPrade, et al. (1975) and others. As a result, stereoscopic viewing is well understood, although there remain unresolved questions.

In binocular vision, the eyes center on a point P (Figure 2), so that a convergence angle γ is subtended. A second point A generates images a', a'' on the retinas, producing a so-called retinal disparity α that leads to observe the point A at a distance different from point P. According to LaPrade, et al. (1975), the retinal disparity angle must at least be 3'' to be observable, and should be smaller than 1° for stereoscopic fusion of the two images. In Nowicki (1966) the minimum retinal disparity is given as 10'' to 20''.

Binocular vision can be simulated by presenting to the eyes two overlapping images of an object. We then speak of *stereoscopic viewing*. We will not discuss the various means or aids to stereoscopic viewing of overlapping images, nor the subjective problems that may arise in visually estimating heights and slopes. These problems have been elaborately treated for camera photography by LaPrade (1973) and others. We will concentrate instead on stereo computations that follow the stereoscopic measurement of radar image coordinates.

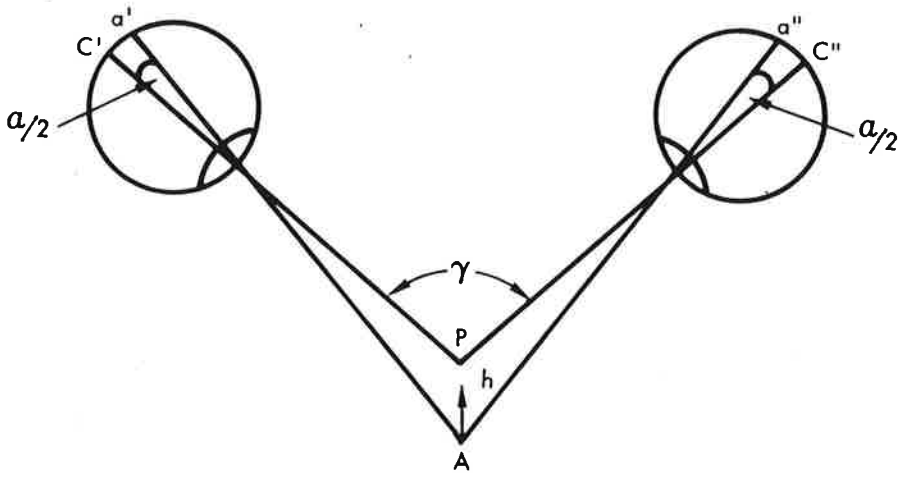

Figure 2. Binocular Vision and Retinal Disparity α
(From LaPrade et al, 1975)

2.2 RADAR STEREO ARRANGEMENTS

The most common radar stereo arrangements are illustrated in Figures 3a, b denoted by *same-side* and *opposite-side*, and obtained in two separate flights or orbits. They were for the first time proposed by LaPrade (1963) and later analyzed by Innes (1964), Rosenfield (1968), LaPrade (1970), Gracie, et al. (1970), Konecny (1972), DBA Systems (1974), Goodyear (1974), Derenyi (1975), Graham (1975, 1976), Leberl (1972, 1975, 1978). An analysis of visual stereo radar perception was attempted by LaPrade (1970), Graham (1975, 1976) and Leberl (1978).

Apart from common same-side and opposite-side arrangements, stereo radar has also been proposed using images taken cross-wise (Leberl, 1972; Graham, 1975), at different altitudes (Leberl, 1972), or in a single flight line or orbit using some sort of convergent scheme (Leberl, 1972; Carlson, 1973; Bair and Carlson, 1974, 1975). These arrangements are illustrated in Figure 4.

Single flight line stereo cannot be realized with synthetic aperture radar (SAR). One may be tempted to believe that in a squinted mode SAR operation (non-zero Doppler correlation) one obtains two stereo looks by once imaging with a positive Doppler frequency (looking forward) and once with a negative frequency (looking backwards). It was pointed out that such arrangements would not produce stereo (Leberl, 1972): Relief displacements would always be at an angle of 90° towards the nadir line, irrespective of the amount of Doppler frequency used for image correlation. As a result there will be zero parallax in squinted SAR image pairs and no valid stereo. An additional outline on this matter is presented in Appendix A.

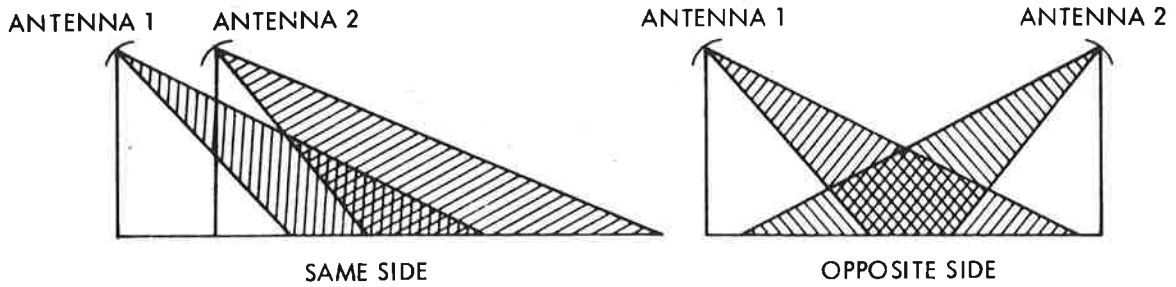

Figure 3. Basic Stereo Radar Arrangements

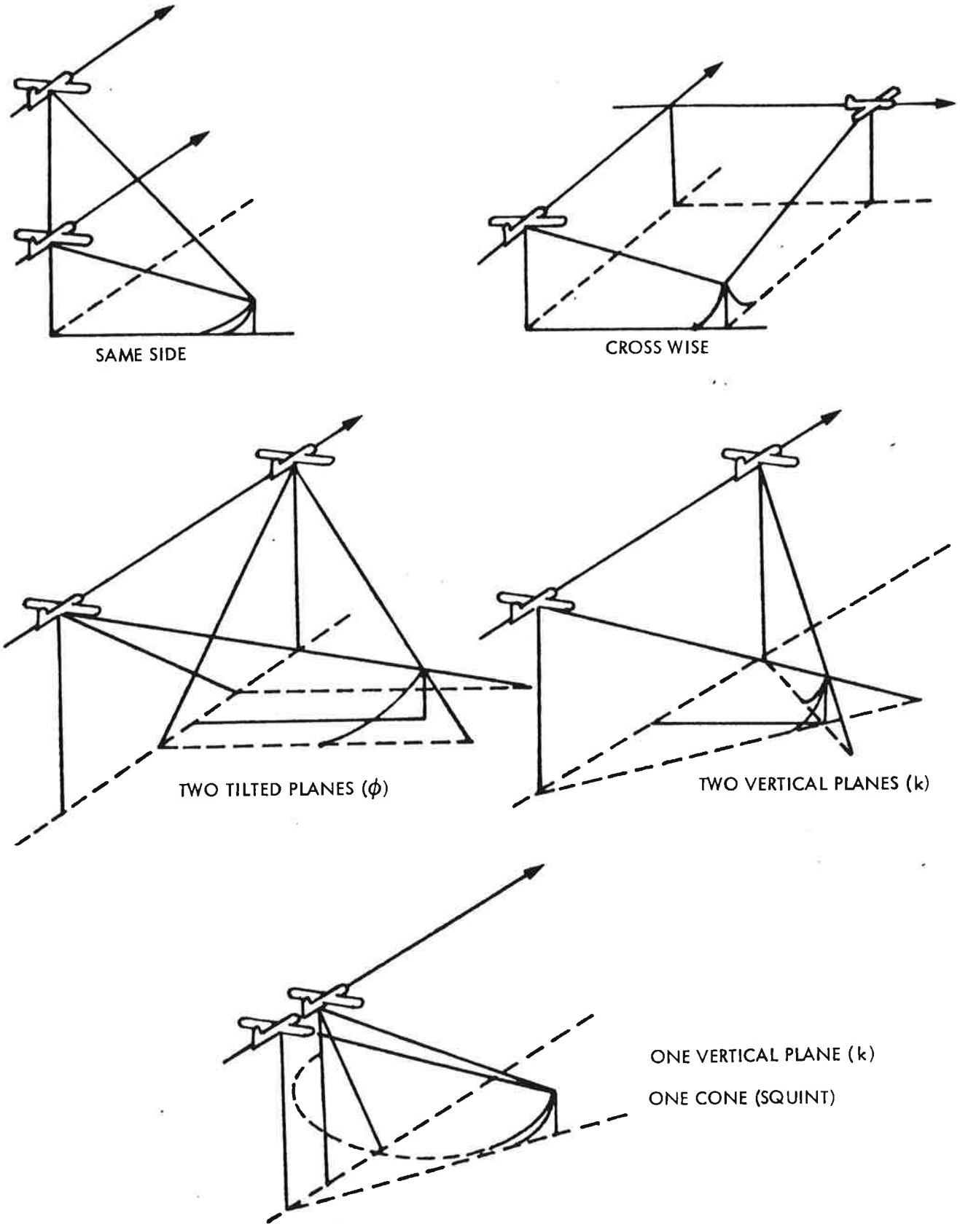

Figure 4. Stereo Arrangements

The single-flight stereo schemes of Figure 4 could be realized with real aperture radar, tilting the radar antennas around horizontal and vertical axes and using conical beams. Since these schemes are invalid with SAR they will not be pursued here.

2.3 FACTORS AFFECTING VISUAL STEREO RADAR

In order to visually perceive a three-dimensional model of the object, the two images of a stereo pair must be sufficiently similar: the image quality, object illumination, tones and textures must be comparable and the geometric differences (stereo parallaxes) must not exceed a value of 1° (retinal disparity). In aerial photography this rarely presents a problem, since sun angles do not change drastically in overlapping photos. However, illumination in the active radar system depends on sensor position. Considerable differences of illumination must therefore be anticipated in radar stereo pairs.

Figures 5 to 8 present examples of radar stereo pairs demonstrating some of the limits to stereo viewing. Figure 5 shows part of the Estrella mountain in Arizona (USA), imaged with an opposite side arrangement from an aircraft at 12 km altitude. It can be observed that slopes reflecting strongly in one image are in the radar shadow in the other image. A stereo impression can be achieved in the flat areas of this stereo pair but becomes impossible in the mountain. Figure 6 demonstrates with a same-side stereo pair that viewing does not present any problems. Koopmans (1973) could show in some tropical areas of Colombia, that this type of same-side radar stereo produced a drainage analysis that was more complete than that from available (poor-quality) aerial photography.

However, there exist also limits to successful same-side stereo. Figures 7 and 8 present two Apollo 17 lunar satellite stereo pairs with same-side geometry and a very small stereo base. Since look angles are steeper than those of Figures 5 and 6, one obtains larger relief displacements and variation of image appearance, even with a small stereo base. In the flat parts of Figure 7, stereo viewing is easy. However, in the Apennin mountains stereo fusion becomes nearly impossible due to the differences of image contents. In the rugged Oriental region of Figure 8 this is even more distinct.

One may thus conclude that radar stereo viewing depends on:

The stereo arrangement;
The look angles off nadir;
The stereo intersection angles;
The ruggedness of the terrain.

In flat or gently rolling areas stereo will hardly present a problem. In rugged terrain, however, stereo is only possible with same-side geometry and improves with shallower look angles. For good visual stereo perception one would prefer small stereo intersection angles: this results in image pairs with little differences in tone and texture, however also in geometry. For good topographic expression (vertical exaggeration) one requires large intersection angles. There exists thus a trade-off between geometric accuracy and ease of perception.

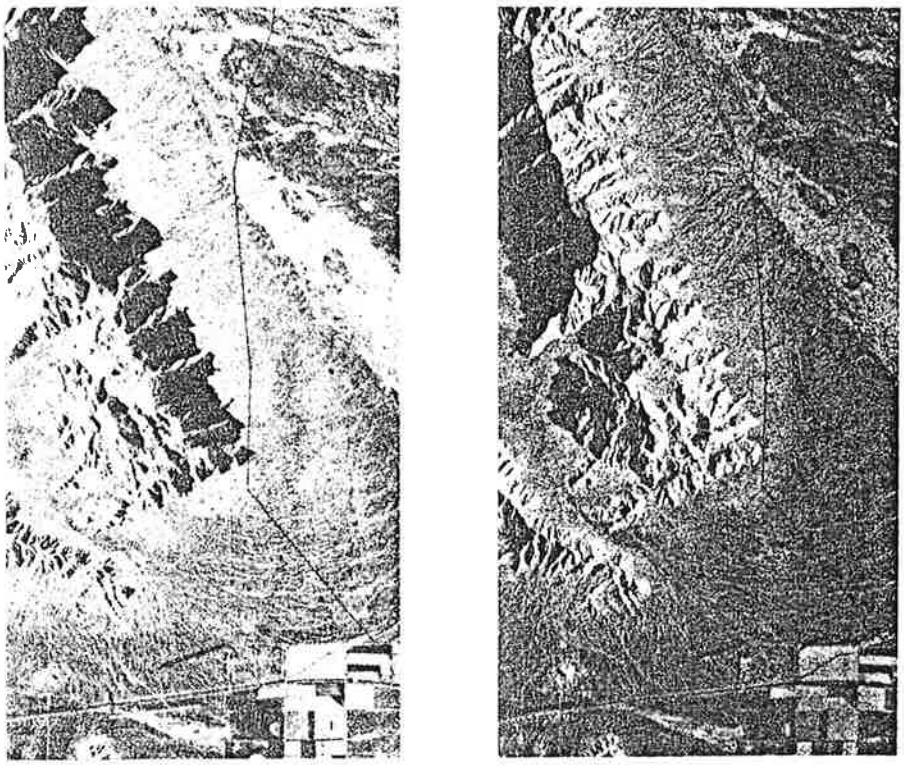

Figure 5. Aircraft Stereo Radar Image Pair, Opposite Side Geometry. X-Band, 12-km Altitude; Estrella Mountains, Arizona (Courtesy of Aeroservice, Goodyear)

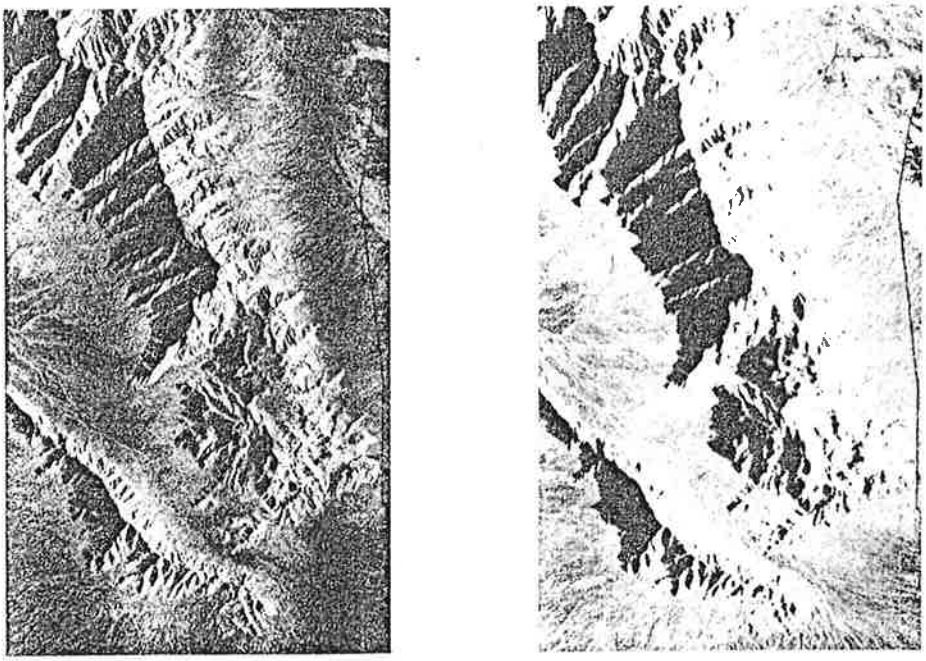

Figure 6. Aircraft Stereo Radar Image Pair, Same Side Geometry. X-Band, 12-km Altitude; Estrella Mountains, Arizona (Courtesy of Aeroservice Goodyear)

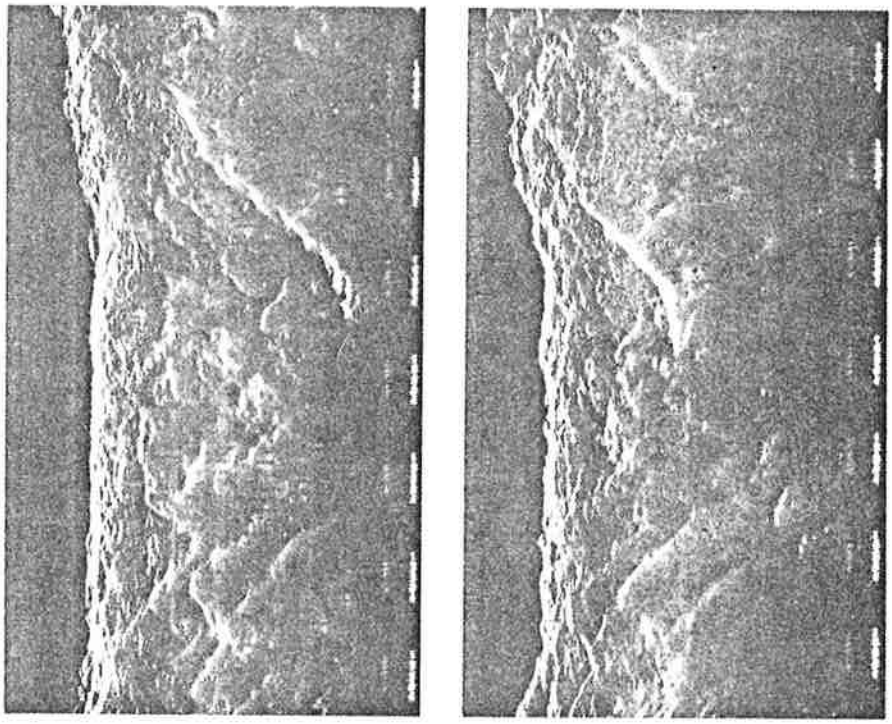

Figure 7. Satellite Stereo Radar, Same Side Imaging Apollo 17 - ALSE-VHF, Apennin on Moon.

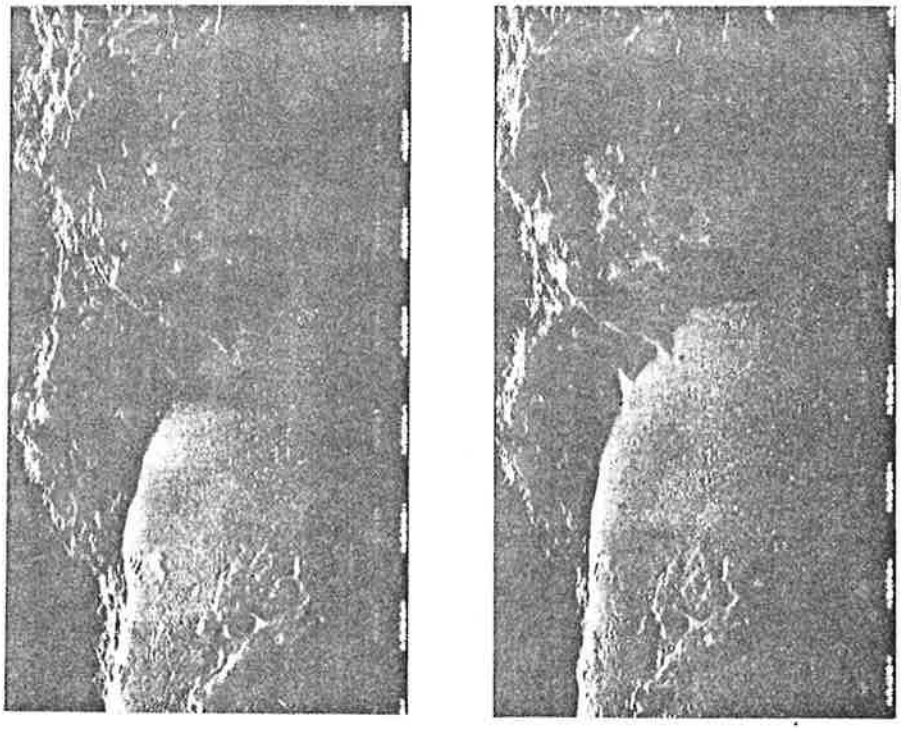

Figure 8. Satellite Stereo Radar, Same Side Imaging, Apollo 17 - ALSE-VHF, Oriental Region on Moon.

For the stereo observation of man-made objects, LaPrade (1975) reports optimum stereo viewing if look angles vary between 37° and 67° off nadir, with intersection angles of about 12° to 15°.

SECTION 3

GEOMETRY OF THE RADAR STEREO MODEL

3.1 GROUND RANGE PRESENTATION

Radar projection lines (lines connecting image and object) are circles that are concentric with respect to the flight line (Figure 1).

If all observed slant ranges are projected on a datum plane then the radar image is in *ground range presentation* (Figure 9). Relief displacement in this case is shown in Figure 10.

Stereo imaging depends on *parallaxes*. One defines *absolute parallax* as shown in Figure 11: the two radar images of a stereo pair are superimposed onto each other in such a way that the flight lines coincide. Absolute parallax then is the distance between the two homologue images A', A'' of an object point A. If an area is flat, and if there is ground range presentation, then all points have the same absolute parallax -- the stereo model appears flat.

Figures 12 and 13 show differences of absolute parallax. These parallax differences may, for example, be measured using a parallax bar and stereoscope, and must then be converted to terrain height differences h. Expressions for this were formulated by Koopmans (1974), Derenyi (1975), Leberl (1975) and others. These expressions use often an approximation by replacing projection circles (wave fronts) by straight lines normal to the *line of sight* connecting object and antenna. The effect of neglecting the curvature of the projection circle reduces with the distance from the antenna and is thus very small for satellite radar.

Formulas to compute height h from radar parallaxes Δp are then, according to Figures 12, 13:

Same Side	Opposite Side
$p' = h \cdot \cot \theta'$	$p' = h \cdot \cot \theta'$
$p'' = h \cdot \cot \theta''$	$p'' = h \cdot \cot \theta''$
$p'' - p' = \Delta p = h (\cot \theta'' - \cot \theta')$	$p' + p'' = \Delta p = h (\cot \theta'' + \cot \theta')$
$h = \Delta p/(\cot \theta'' - \cot \theta')$	$h = \Delta p/(\cot \theta' + \cot \theta'')$

(1)

Practical application of formulas (1) depends on the knowledge of look angles θ', θ''. We see that these vary for each image point. Also, they are only approximately known, since not the angle to point P is available, but the angles to points P', P''.

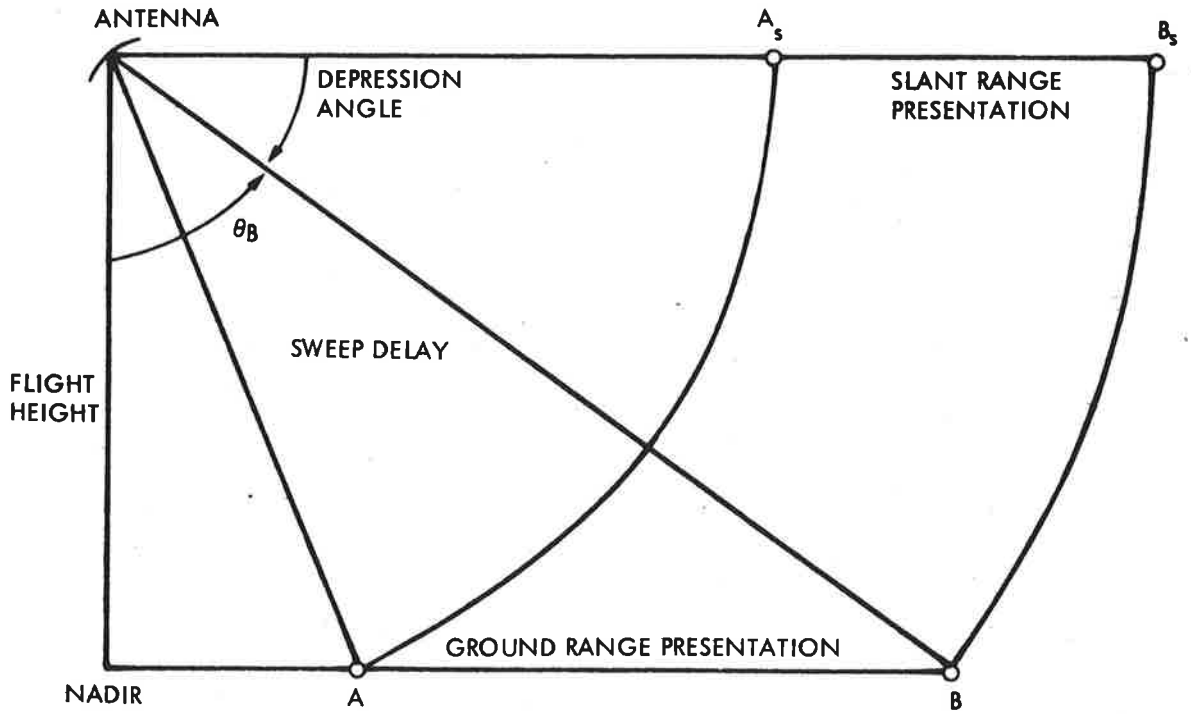

Figure 9. Radar Image Presentations

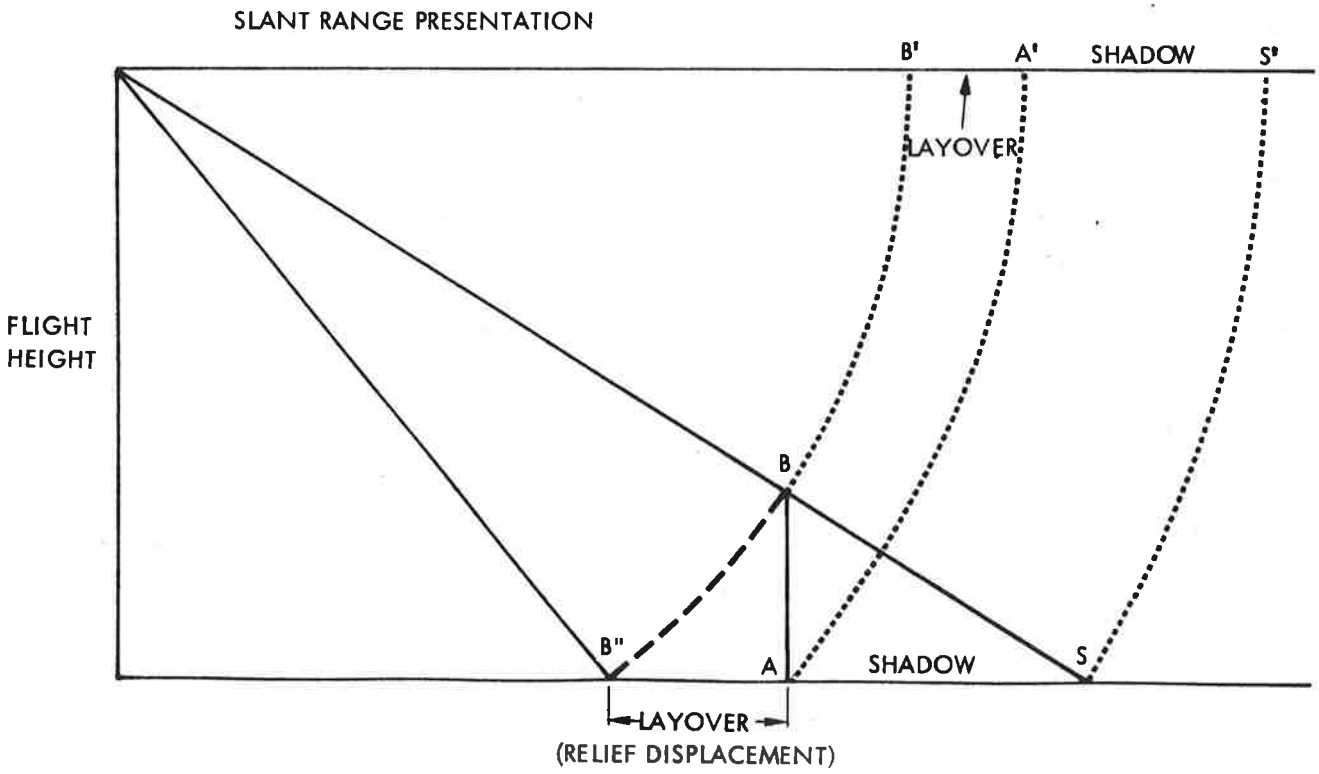

Figure 10. Radar Relief Displacement

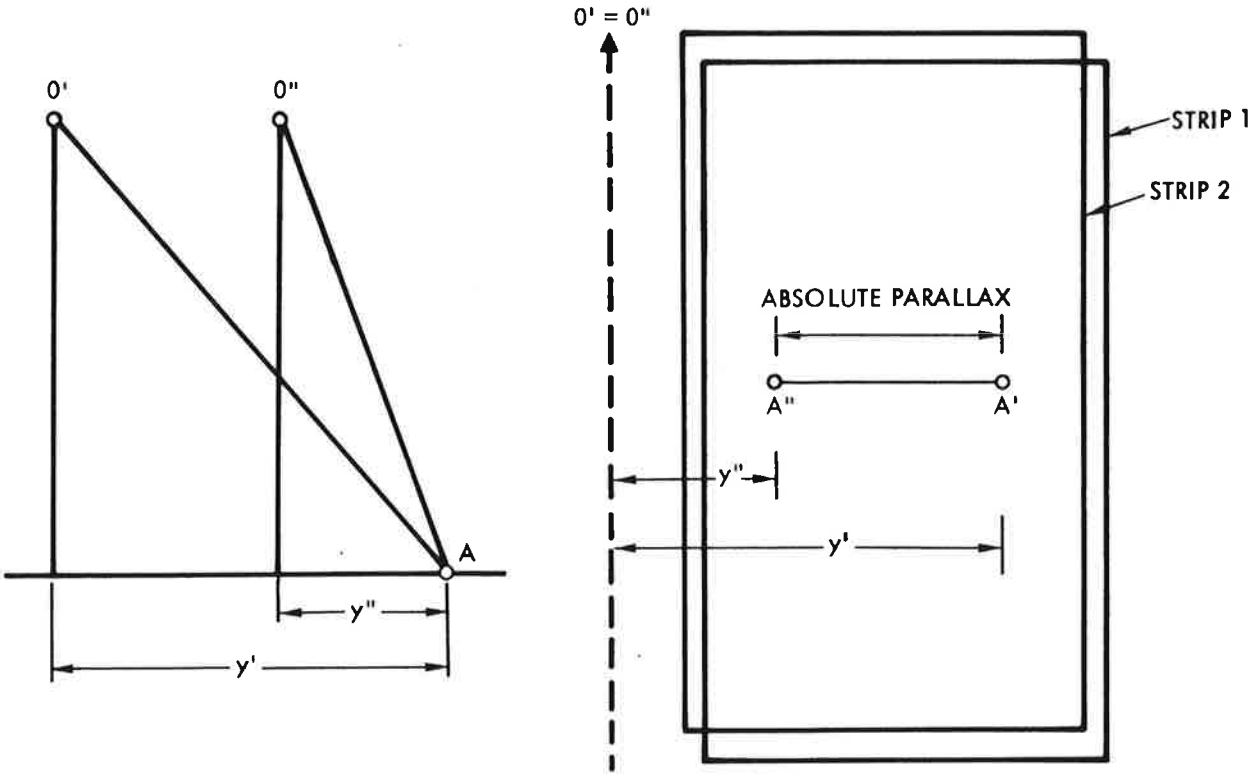

Figure 11. Definition of Absolute Parallax

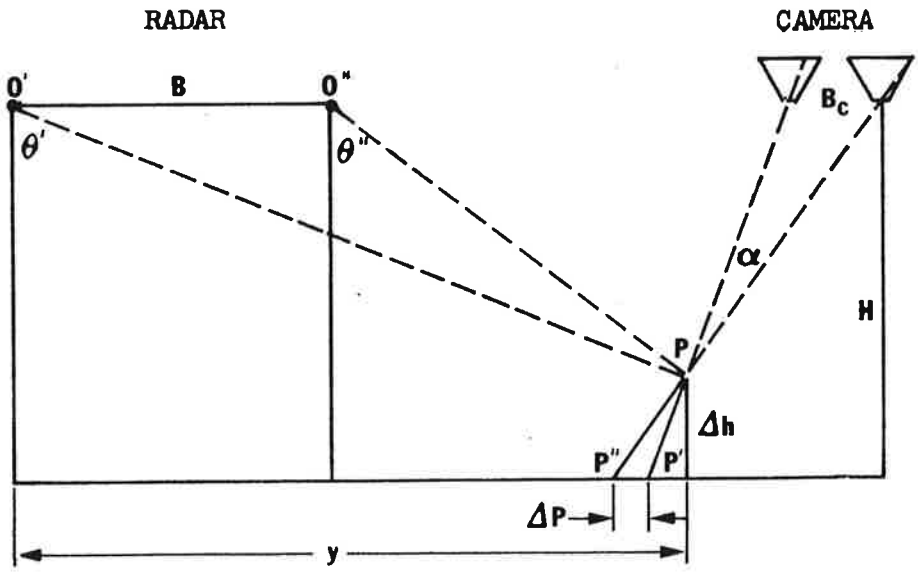

Figure 12. Stereo Radar Parallaxes, Same Side Geometry. Shown is also the camera arrangement to obtain the same parallax (LaPrade, 1970).

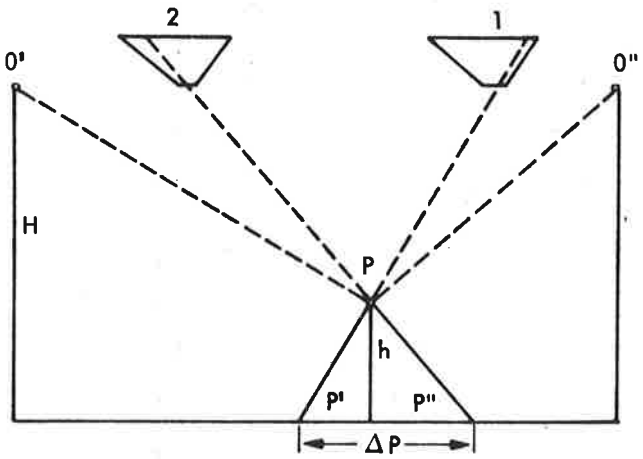

Figure 13. Stereo Radar Parallaxes, Opposite Side Geometry. Shown is also the camera arrangement to obtain the same parallax (LaPrade, 1970).

Expressions (1) are the radar equivalent of the simple photogrammetric parallax formula:

$$h = \Delta p \cdot H/B$$

as used in photointerpretation.

It may be significant to point out that in photography object heights h will be directly proportional to parallax difference Δp, involving merely a constant proportionality factor H/B. With radar, however, parallax differences Δp produce different heights h, depending on the look angles θ', θ''.

3.2 SLANT RANGE PRESENTATION

A single slant range radar presentation generates a panoramic visual impression as illustrated in Figure 14 and confirmed in the images of Figures 8 and 9. Also a stereo-image pair creates a bowed stereo model. For slant range

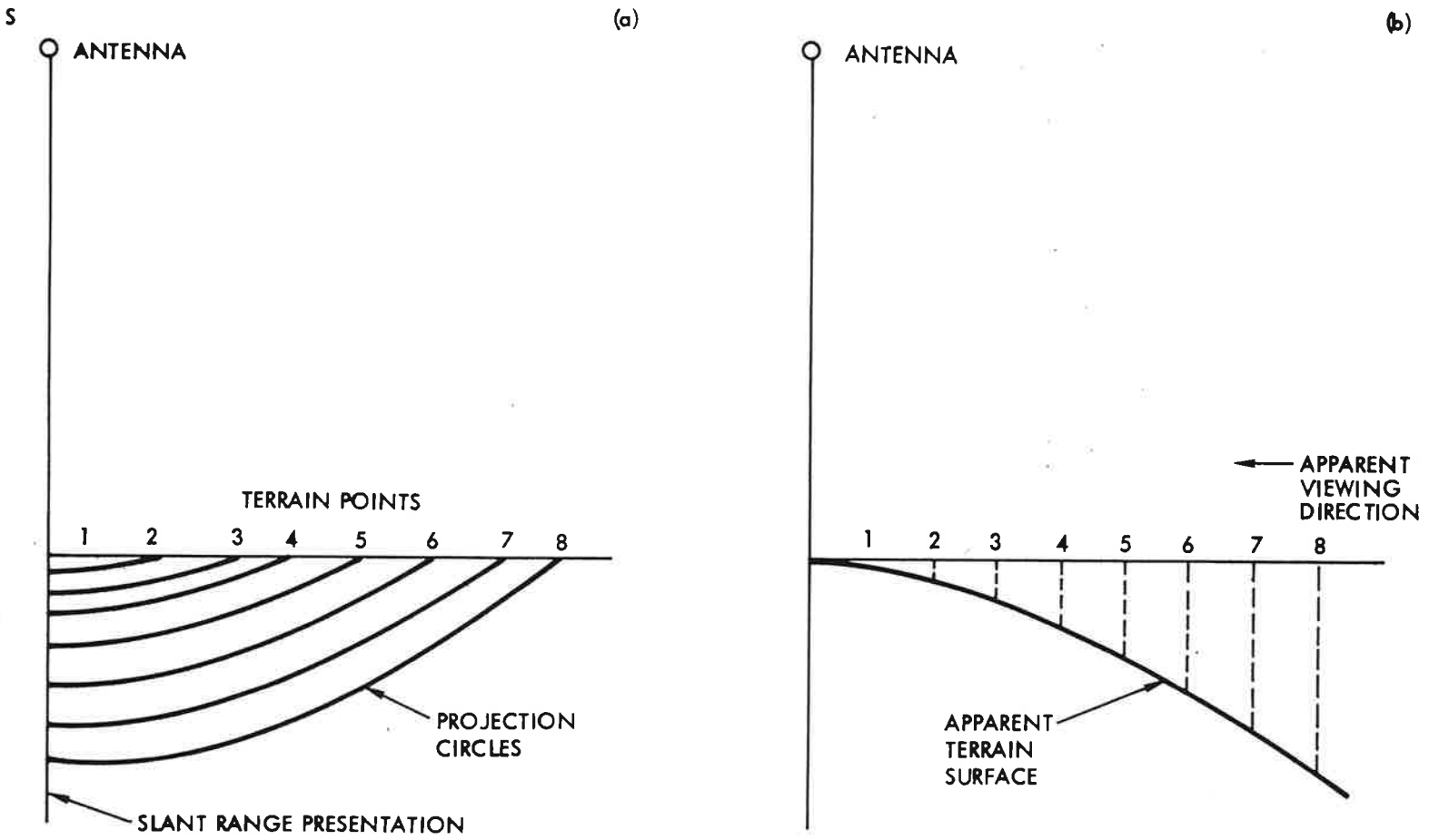

Figure 14. Visual Impression Obtained from Slant Range Presentation

presentations, one seems to have to deal with a more complex situation, since the absolute parallax is variable even for points in the datum plane.

The absolute parallax p must be defined as:

$$p = r' - r'' \tag{2}$$

where r', r'' are slant ranges to an object point, measured in images (1), (2), respectively. From Figure 15 we know that:

$$r' = (H^2 + y^2)^{1/2}$$

$$r'' = (H^2 + (y-B)^2)^{1/2}$$

so that

$$p = (H^2 + y^2)^{1/2} - (H^2 + (y-B)^2)^{1/2} \tag{3}$$

The absolute parallax depends on the value of y. It can be shown that the relationship between p and y defines a *super-hyperbolic* cylinder in the x,y,p - space (Leberl, 1978). One can verify, that for y = B/2, p = 0; for y > B/2, p > 0; for y < B/2, p < 0. These facts are illustrated in Figure 15 and clearly present the super-hyperbolic cylinder of flat terrain. Relief is on top of the cylinder. According to Figure 16 the height h above the super-hyperbolic cylinder results from:

$$p' = h \cdot \cos \theta'$$

$$p'' = h \cdot \cos \theta''$$

$$h = \Delta p/(\cos \theta' \pm \cos \theta'') \tag{4}$$

Where the minus sign is for same-side, the plus sign for opposite-side arrangements.

3.3 RIGOROUS STEREO INTERSECTION

Rigorous radar stereo intersection algorithms were used by Gracie, et al. (1970), DBA-Systems (1974), Leberl (1976), and for underwater SONAR images by

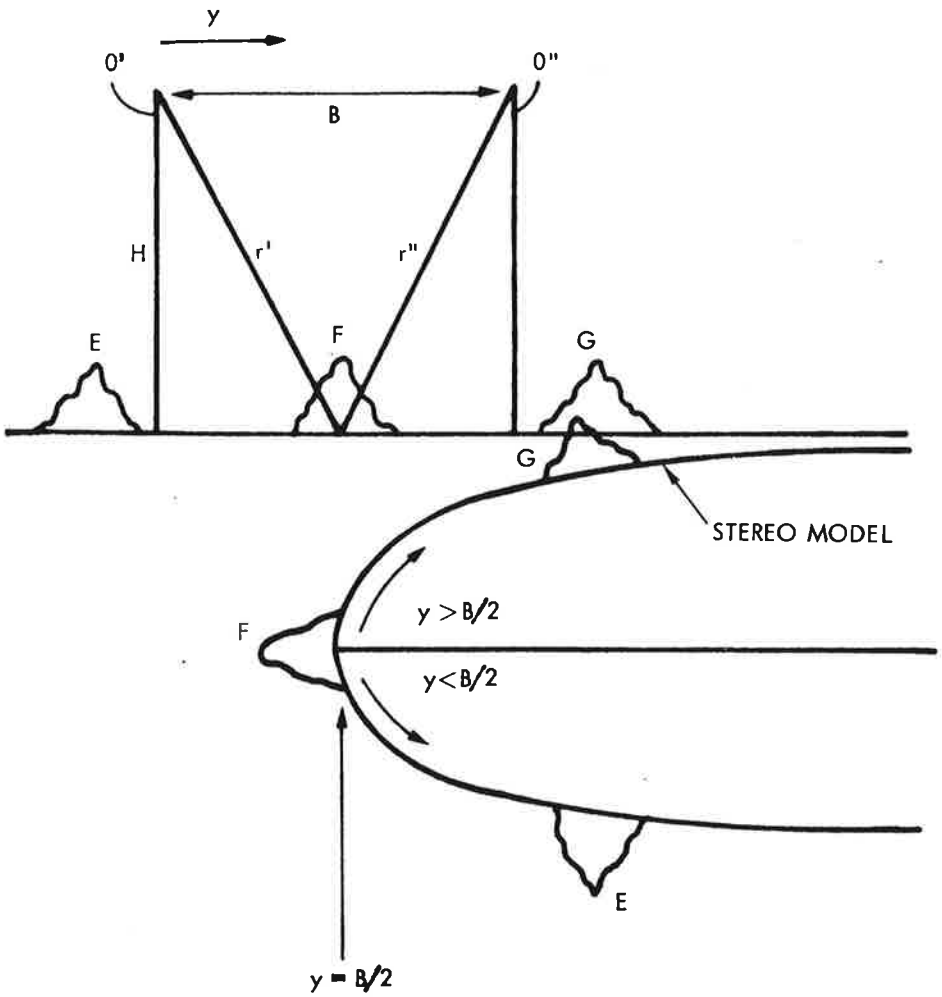

Figure 15. Stereo in Slant Range Presentation, Terrain Rolled onto Cylinder

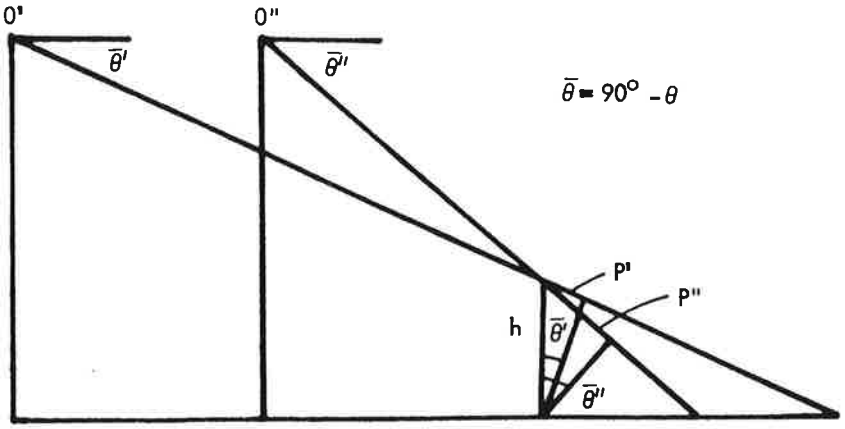

Figure 16. Height Differences in Slant Range Presentation

Clerici and Konecny (1978). These formulations define a position vector $\underline{p}$ for an object point P, using all available information on sensor position $\underline{s}$, attitude $\dot{\underline{s}}$ (velocity vector), squint angle τ, slant range r. Figure 17 illustrates the situation:

$$\underline{p} = \underline{s}' + \underline{r}'$$
$$\underline{p} = \underline{s}'' + \underline{r}'' \qquad (5)$$

or (from Leberl, 1976):

$$|\underline{p} - \underline{s}'| = r' \qquad (a)$$
$$|\underline{p} - \underline{s}''| = r'' \qquad (b)$$
$$\dot{\underline{s}}' \cdot (\underline{p} - \underline{s}') = \sin\tau(|\dot{\underline{s}}'||\underline{p} - \underline{s}'|) \qquad (c) \qquad (6)$$
$$\dot{\underline{s}}'' \cdot (\underline{p} - \underline{s}'') = \sin\tau(|\dot{\underline{s}}''||\underline{p} - \underline{s}''|) \qquad (d)$$

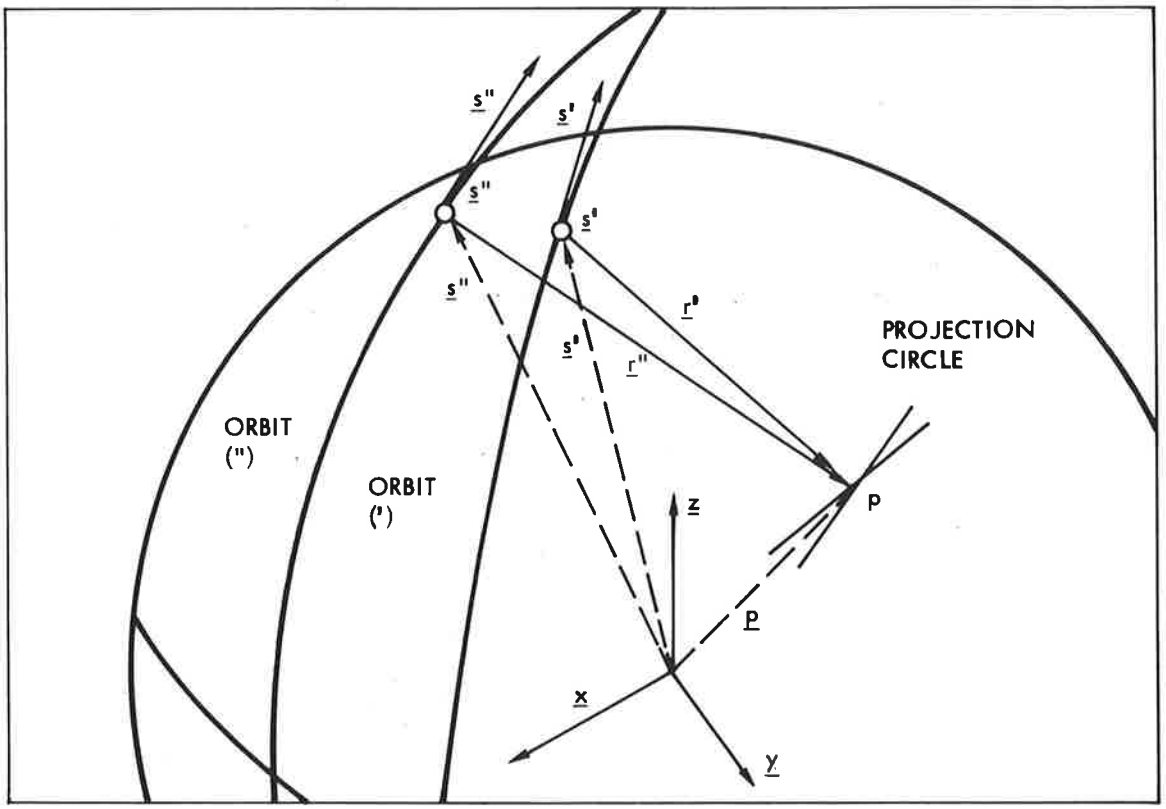

Figure 17. Rigorous Stereo Intersection

where Equation (6) presents the two range spheres (a) and (b) and Doppler cones (c) and (d). The elements of vector $\underline{p}$ are unknown. Since 4 equations exist for 3 unknowns, an adjustment can be carried out. The algorithm for this is listed in Appendix B.

SECTION 4

VERTICAL EXAGGERATION IN STEREO RADAR

LaPrade (1970) and Graham (1976) have discussed vertical exaggeration in radar stereo models. These considerations relate the radar stereo parallax to the base to height ratio B_c/H of equivalent camera photography as shown in Figures 12, 13. From these figures it is obvious that for ground range presentations (compare Equation (4) with $B_c/H = \Delta p/h$):

$$B_c/H = \cot \theta' - \cot \theta'' \tag{7}$$

and for slant range presentation (compare Equation (4)):

$$B_c/H = \cos \theta' - \cos \theta'' \tag{8}$$

where B_c is the stereo base of the equivalent camera arrangement.

The ratio B_c/H is a measure of *vertical exaggeration* q that has been extensively analyzed in photogrammetry. The factor q can be defined as the ratio between the true height-to-base-ratio h/b of an object and its visually perceived stereo model equivalent, h_i/b_i:

$$q = (h \cdot b_i)/(h_i \cdot b) \tag{9}$$

Following LaPrade (1972), the factor q for photography is found to be:

$$q \approx 5 \cdot B_c/H \tag{10}$$

if the stereo-model is observed in a stereoscope and if the separation of photographs produces an angle γ of 0.20 radians (γ as defined in Figure 12).

One obtains then as the vertical exaggeration of stereo radar:

$$q \approx 5(\cot \theta' - \cot \theta'') \tag{11}$$

or, as shown by Graham (1976) and deriving from Figure 12:

$$q \approx 5 \cdot H \cdot B/\{y(y - B)\} \tag{12}$$

Figure 18 presents the values for q for airborne radar and the proposed VOIR orbital mission. For the optimum stereo radar arrangement as defined by LaPrade (1975), we find (compare Section 2.3):

$$37^\circ < \theta' < 67^\circ$$

$$12^\circ < \Delta\theta < 15^\circ$$

where

$$\Delta\theta = \theta' - \theta'' .$$

Therefore

$$2.3 > q > 1.8 .$$

These values for q are smaller than what one would obtain with wide-angle photography, where B/H = 0.6, so that:

$$q = 3 .$$

It is also obvious that q is variable across a radar stereo model while for photography it is a constant for a given stereo pair.

For VOIR, vertical exaggeration must be expected to only amount to $q \approx 0.6$, since stereo intersection angles are small: $3^\circ.3 > \Delta\theta > 2^\circ.8$.

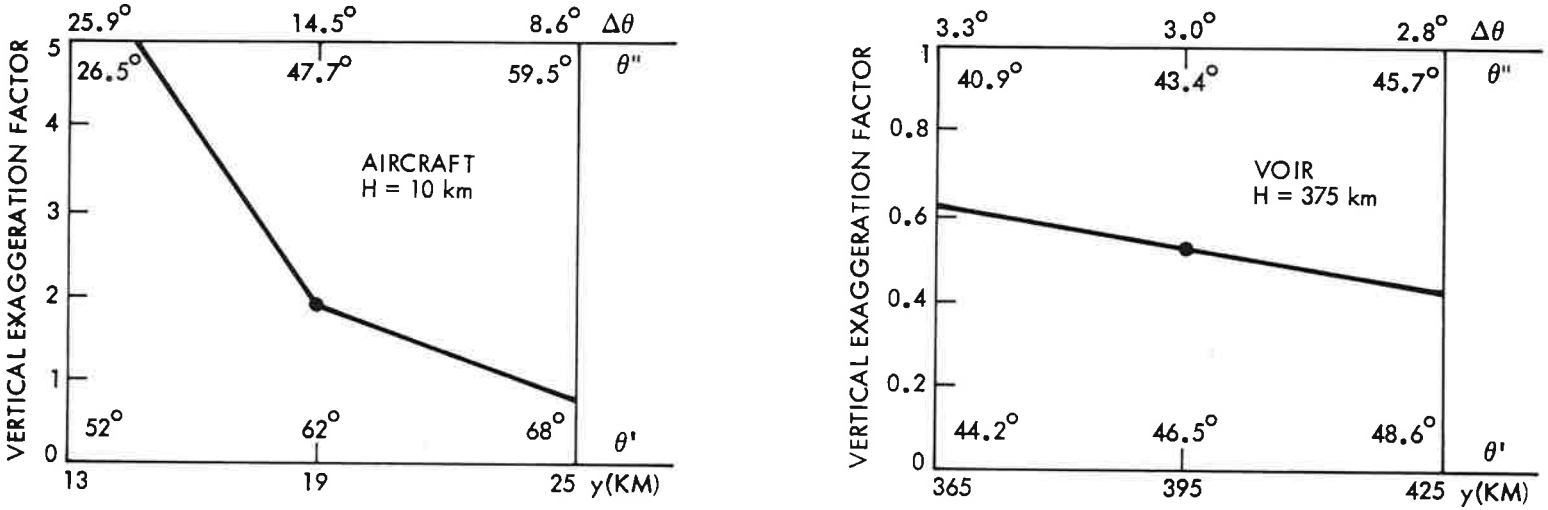

Figure 18. Vertical Exaggeration Factor q for Aircraft and VOIR-Stereo Radar. The value of q varies from near to far range

SECTION 5

ERRORS OF THE RADAR STEREO MODEL

Errors of the radar stereo model should be divided into two groups: *absolute errors* are errors of individual point coordinates, or planetocentric, positions and height. *Relative errors* are those of coordinate differences.*

Error analyses have been previously published by Rosenfield (1968), LaPrade (1970) and Leberl (1972) for airborne radar, and by Leberl (1978) for satellite radar. These analyses were limited, e.g., to compare same-side with opposite-side stereo, and addressed only absolute errors. The present analysis aims at a more general approach, identifying both absolute and relative errors irrespective of flight arrangement.

Figure 19a defines absolute errors that result from errors of the orbit positions $\underline{s}'$, $\underline{s}''$; of the velocity vectors $\underline{\dot{s}}'$, $\underline{\dot{s}}''$; of slant ranges r', r'', while Figure 19b shows how a pair of points with absolute errors combines to define relative errors.

One is dealing with error vectors $\underline{ds}'$, $\underline{ds}''$, $\underline{d\dot{s}}'$, $\underline{d\dot{s}}''$ and with dr', dr''.

5.1 COORDINATE ERRORS

For the derivation and discussion of errors of the radar stereo model, a coordinate system and flight arrangement as shown in Figure 20 are used, where:

$$\begin{aligned} \underline{s}' &= (x_o', y_o', z_o') = (0, 0, H) \\ \underline{\dot{s}}' &= (\dot{x}_o', 0, 0) \\ \underline{s}'' &= (x_o'', y_o'', z_o'') = (0, B, A) \\ \underline{\dot{s}}'' &= (\dot{x}_o'', 0, 0) \end{aligned} \qquad (13)$$

*Relative errors are often used as defined here. Correctly, however, this term should be used only for the ratio of error and observed quantity and be expressed in percent (%).

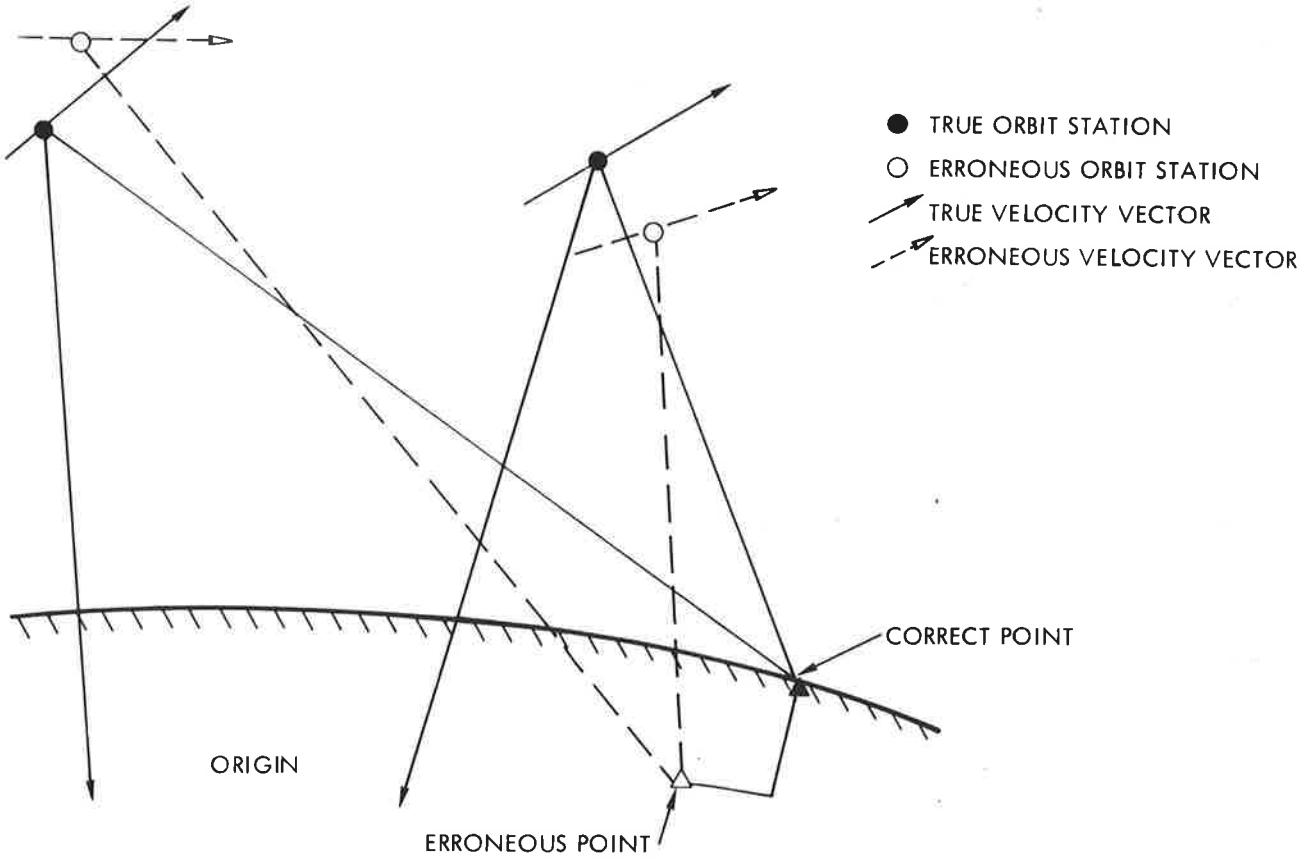

Figure 19. (a) Absolute Errors of Stereo Model

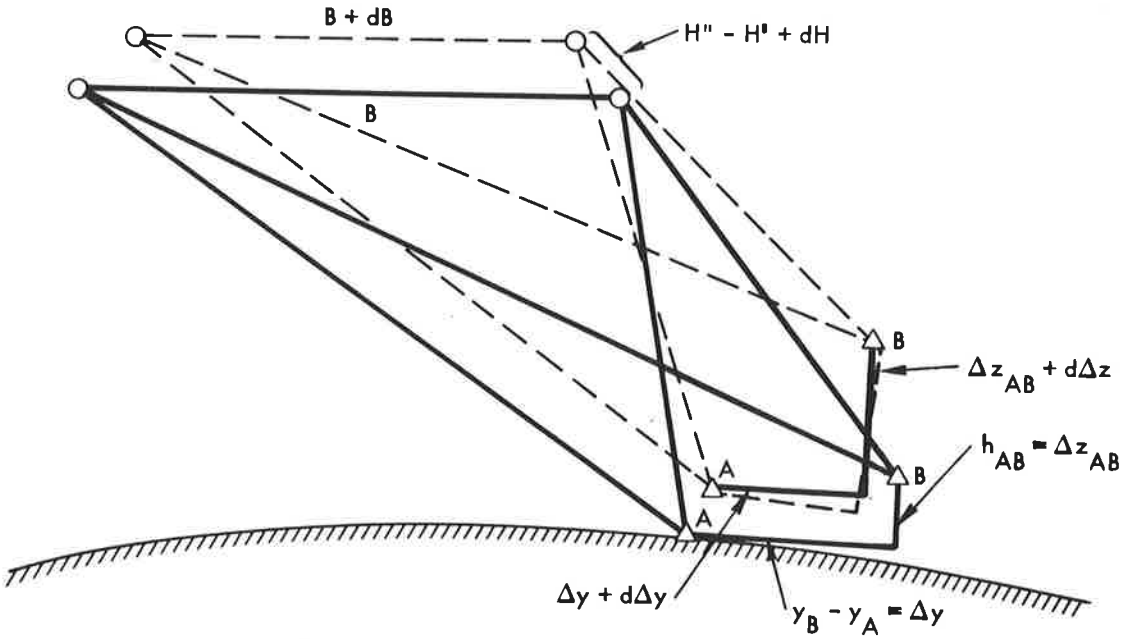

Figure 19. (b) Relative Errors $d\Delta y$, $d\Delta z$ of Stereo Model

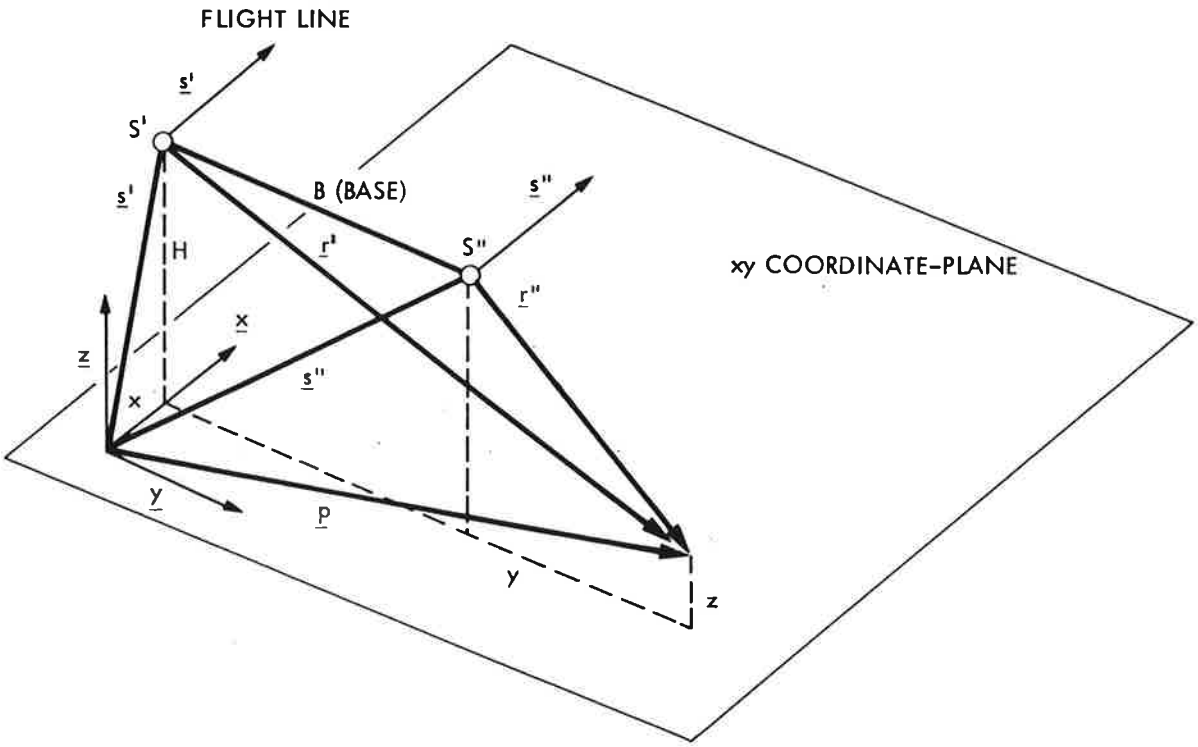

Figure 20. Coordinate System

It is obvious to see that an error dx_o' has no effect on y and z, so that:

$$dx_{xo}' = dx_o'/2, \qquad dx_{xo}'' = dx_o''/2,$$

$$dy_{xo}' = 0 \quad , \qquad dy_{xo}'' = 0 \quad , \tag{14}$$

$$dz_{xo}' = 0 \quad , \qquad dz_{xo}'' = 0 \quad .$$

The effects of dy_o', dy_o'' are less obvious. Figure 21 clarifies the relationship. There is no effect on x. In y, we find:

$$\frac{dy}{\ell} = \frac{H}{r'}$$

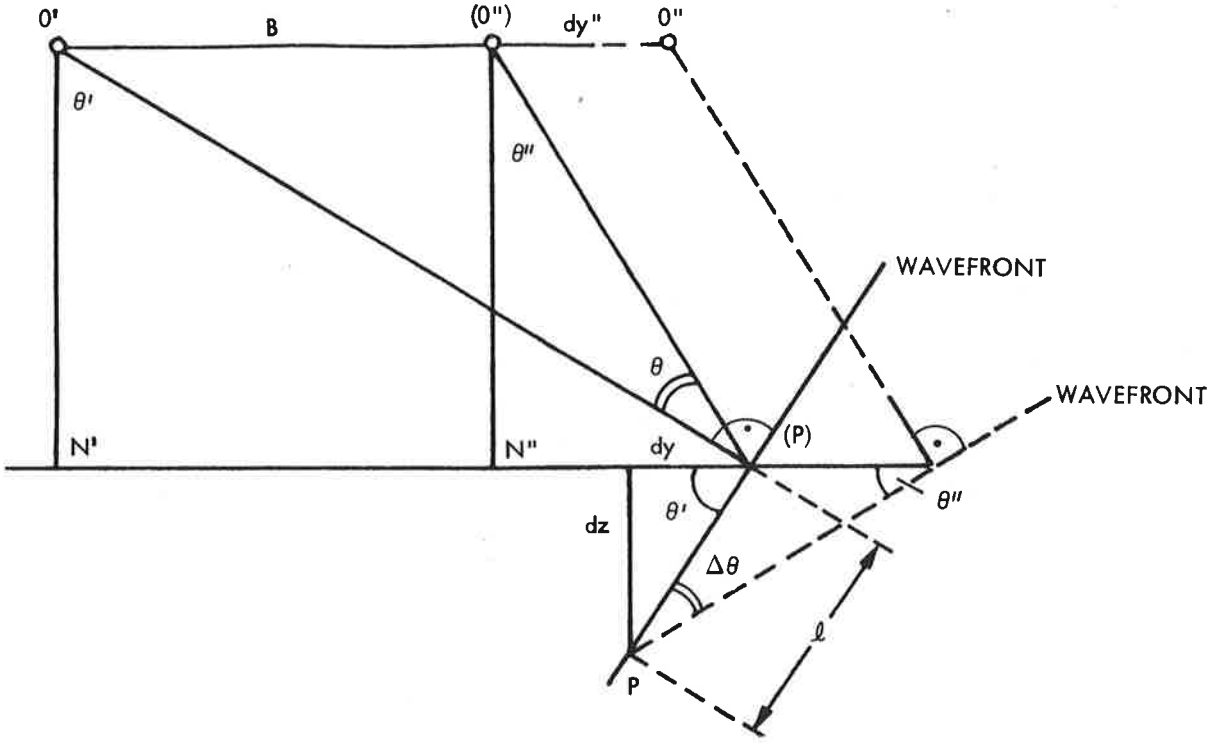

Figure 21. Errors Due to y_o''-Component of Sensor Position

with

$$\frac{\ell}{dy_o''} = \frac{\sin \theta''}{\sin (\theta' - \theta'')}$$

So that:

$$dy = H \cdot dy_o'' \sin \theta''/(r' \sin (\theta' - \theta'')) \qquad (15)$$

But:

$$\frac{r'}{B} = \frac{\sin (90^\circ - \theta'')}{\sin (\theta' - \theta'')}$$

$$r' \sin (\theta' - \theta'') = B \sin (90^\circ - \theta'') \qquad (16)$$

Introducing (16) in (15) gives:

$$dy = dy_o'' \, H \tan \theta''/B$$

so that, finally:

$$dy_{yo}'' = dy_o'' \, (B-y)/B \qquad (17)$$

We can substitute for y/B also:

$$\frac{y}{B} = \frac{y}{r'} \cdot \frac{r'}{B} = \frac{\sin \theta' \sin (90^\circ + \theta'')}{\sin (\theta' - \theta'')} = \frac{1}{1 - \cot \theta' \tan \theta''}$$

A similar development can be found for dz_{yo}'', so that we obtain:

$$dx_{yo}'' = 0$$

$$dy_{yo}'' = dy_o'' \, (B - y)/B = dy_o''/(1 + \cot \theta' \tan \theta'')$$

$$dz_{yo}'' = dy_o'' \, y(y - B)/H \, B = -dy_o''/(\cot \theta'' - \cot \theta')$$

and similarly for the other sensor station: (18)

$$dx_{yo}' = 0$$

$$dy_{yo}' = dy_o' \cdot y/B = dy_o'/(1 - \cot \Omega' \tan \Omega'')$$

$$dz_{yo}' = dy_o' \cdot y \cdot (y - B)/(H \cdot B) = dy_o'/(\cot \theta'' - \cot \theta')$$

Equations (18) show that the y-dimension of the stereo model is deformed linearly; this is a scale error. The model height is deformed linearly in y, representing a model tilt, and in addition there is a nonlinear model bow due to the y^2-term. Error curves are presented in Appendix C.

The effects of height errors dz_o', dz_o'' are shown in Figure 22. A derivation like the one for Equation 18 results in

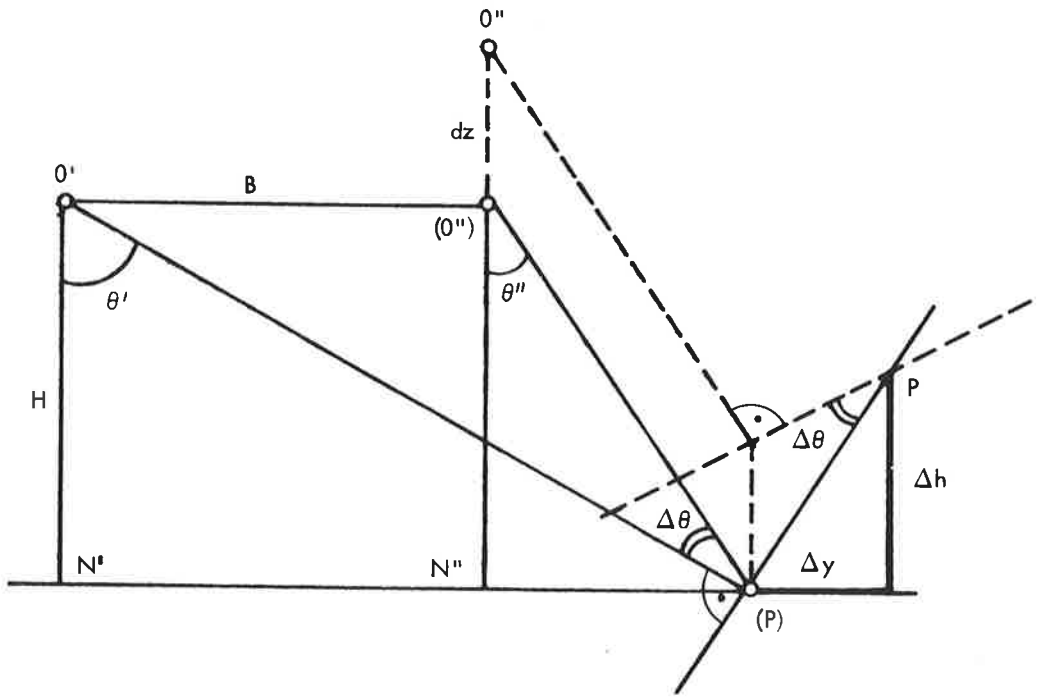

Figure 22. Errors Due to z_o''-Component of Sensor Position

$$
\begin{aligned}
dx_{zo}' &= 0 \\
dy_{zo}' &= -dz_o' \, H/B = dz_o'/(\tan\theta'' - \tan\theta') \\
dz_{zo}' &= -dz_o' \, (y - B)/B = dz_o'/(1 - \tan\theta' \cot\theta'') \\
dx_{zo}'' &= 0 \\
dy_{zo}'' &= dz_o'' \, H/B = dz_o'/(\tan\theta' - \tan\theta'') \\
dz_{zo}'' &= dz_o'' \, Y/B = dz_o'/(1 - \cot\theta' \tan\theta'')
\end{aligned}
\qquad (19)
$$

An error of sensor altitude does not deform the model y-dimension, but merely shifts the model in y. In height, there is a linear effect of model tilt. Error curves are shown in Appendix C.

Erroneous sensor attitudes, caused by errors of the velocity vectors $\underline{\dot{s}}'$, $\underline{\dot{s}}''$, lead to nonintersecting projection circles. This is illustrated in Figure 23, for the example of an error $d\dot{y}_o'$ which creates an antenna swing k. We need to define a model point, that most logically is chosen halfway between the error-free point obtained if no $d\dot{y}_o'$ error had been present.

From Figure 23 we find that an error $d\dot{y}_o'$ affects the x-coordinates of the model point P, shifting it to position $\bar{p}$, but leaves the y,z-coordinates unchanged, at least to a first-order approximation:

$$
\begin{aligned}
dx_{\dot{y}o}' &= d\dot{y}_o' \cdot y/2 = d\dot{y}_o' \cdot H \cdot \tan\theta'/2, \\
dy_{\dot{y}o}' &= 0, \\
dz_{\dot{y}o}' &= 0, \\
dx_{\dot{y}o}'' &= d\dot{y}_o'' \, (y - B)/2 = d\dot{y}_o'' \cdot H \cdot \tan\theta''/2, \\
dy_{\dot{y}o}'' &= 0, \\
dz_{\dot{y}o}'' &= 0.
\end{aligned}
\tag{20}
$$

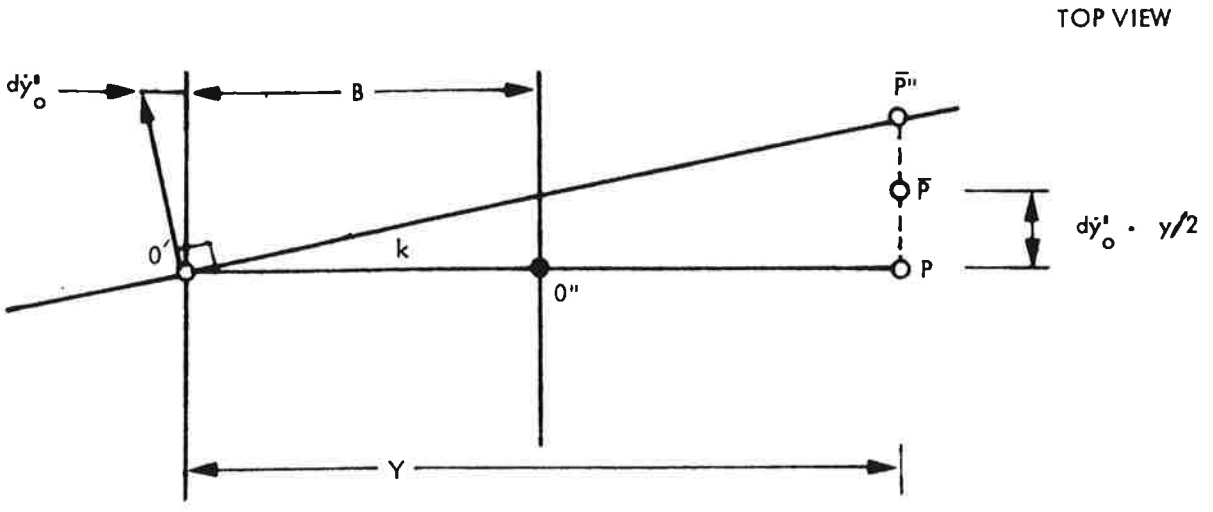

Figure 23. Error Due to $d\dot{y}_o$ -Component of Velocity Vector

Similarly, the $d\dot{z}_o'$, $d\dot{z}_o''$-components cause a tilt ϕ of the radar antenna, so that:

$$
\begin{aligned}
dx_{\dot{z}o}' &= d\dot{z}_o' \cdot H/2, \\
dy_{\dot{z}o}' &= 0, \\
dz_{\dot{z}o}' &= 0, \\
dx_{\dot{z}o}'' &= d\dot{z}_o'' \cdot H/2, \\
dy_{\dot{z}o}'' &= 0, \\
dz_{\dot{z}o}'' &= 0.
\end{aligned}
\tag{21}
$$

An erroneous $d\dot{x}_o'$, $d\dot{x}_o''$-component will not affect the antenna attitude and thus not produce errors of the stereo model. It will, of course, affect antenna position when integrated over time. This error was considered in Equation (14).

A last error of the stereo-model results from erroneous range data r', r''. Figure 24 shows that:

$$
\begin{aligned}
dx_r' &= 0 \\
dy_r' &= dr' \cdot r'/B = dr' (y^2 + H^2)^{1/2}/B = dr' \cdot \cos\theta''/\sin(\theta' - \theta'') \\
dz_r' &= dr' \cdot r' \cdot (y - B)/B \cdot H = dr' \sin\theta''/\sin(\theta' - \theta'') \\
dx_r'' &= 0 \\
dy_r'' &= -dr'' \cdot r''/B = -dr'' \cdot \cos\theta'/\sin(\theta' - \theta'') \\
dz_r'' &= -dr'' \cdot y \cdot r''/BH = -dr'' \sin\theta'/\sin(\theta' - \theta'')
\end{aligned}
\tag{22}
$$

These errors are nonlinear in the y and z-dimensions. Error curves are plotted in Appendix C.

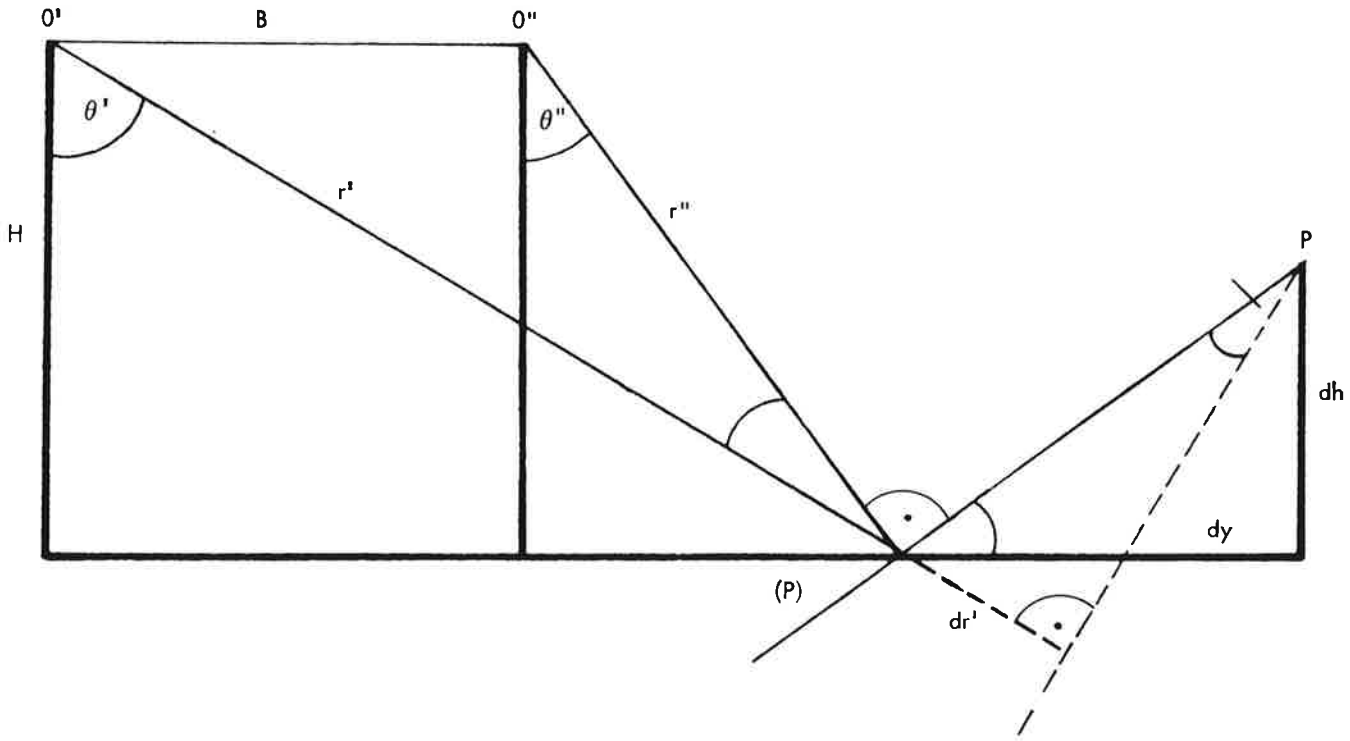

Figure 24. Error Due to Range Error

5.2 ERRORS OF COORDINATE DIFFERENCES

Coordinate errors generally are of lesser importance than are errors of coordinate differences -- these are actually the entities that are to be derived from stereo radar. In this context it is legitimate to study only the effects of an error of dB of the stereo base B, of erroneous height differences dH between the two antenna positions, and of range errors dr´, dr´´. The along track model dimension is not affected by dB, dH, dr´, dr´´ (compare Equation 18, 19, 20). Therefore, it is of little concern in a stereo-radar analysis.

5.2.1 Stereo Base: dB

The *errors of coordinate differences* in cross track and height are denoted by $d\Delta y$, $d\Delta z$. They follow from partially differentiating the following equations for the *coordinate errors*, using $dB = dy_o'' - dy_o'$ (compare Eqn. (18)):

$$dy_B = \frac{-y}{B} dB + \text{const.}$$
$$dz_B = \frac{B - y}{BH} y\, dB \qquad (23)$$

The partial derivative with respect to y and z produces the following equation for the errors $d\Delta y$, $d\Delta z$ of coordinate differences:

$$d\Delta y_B = \left\{ -\frac{\Delta y}{B} \right\} dB \qquad (24a)$$

$$d\Delta z_B = \left\{ \left(\frac{1}{H} - \frac{2y}{B \cdot H} \right) \Delta y - \frac{y \cdot (B - y)}{B\, H^2} \Delta z \right\} dB \qquad (24b)$$

Equations (24) describe the change of coordinate errors with varying the model coordinates y and z. It is to be noted that the model height z and flight height H complement each other, so that with the definitions of Figure 20 $dH = dz$ and $\Delta H = \Delta z$.

Equations (24) are valid for small values of Δy, Δz -- they refer to errors deforming small coordinate differences Δy, Δz in model space. Conclusions to be drawn from Equations (24) are evident:

- Cross-track distances have errors directly proportional to base-errors.
- Height differences have a more complex error behaviour; for vertical structures ($\Delta y = 0$) errors increase with both a linear and a non-linear term in y.
- Heights measured of points that are spaced apart for Δy have errors that consist of a small constant term and a large term growing linearly with y.

Numerical examples are presented in Appendix C.

5.2.2 Flight Altitude: dH

We start out from Equations (19), denoting by $dH = dz_o'' - dz_o'$. This leads to:

$$dy_H = \frac{H}{B} dH$$

$$dz_H = \frac{y}{B} dH + \text{const} \qquad (25)$$

These equations, when partially differentiated, lead to:

$$d\Delta y_H = \frac{dH}{B} \Delta z \qquad (26a)$$

$$d\Delta z_H = \frac{dH}{B} \Delta y \qquad (26b)$$

We find here a simple error situation: cross track distances and height differences have errors that are directly proportional to dH/B, where cross track distances have errors only if end points are at different altitudes, and heights of vertical structures would be error-free.

5.2.3 Range Errors: dr', dr''

Range errors may be of two origins:

(a) Limited range resolution causes random errors of range measurement.

(b) Errors of range calibration, measurement etc. may lead to systematic range deformations.

Range resolution defines the *height definition*, thus the accuracy with which we can set a mark on the surface of the observed stereo model. Similarly, also the y-coordinate is subject to a limited definition.

An expression is easily found for the cross-track and height definition starting from Equations (22), where the random errors of height and cross-track coordinate result from error propagation and are denoted by:

$$\sigma_y = \sigma_i \left\{ \cos^2 \theta' + \cos^2 \theta'' \right\}^{1/2} / \sin (\theta' - \theta'') \qquad (27a)$$

$$\sigma_z = \sigma_i \left\{ \sin^2 \theta' + \sin^2 \theta'' \right\}^{1/2} / \sin (\theta' - \theta'') \qquad (27b)$$

or:

$$\sigma_y = \sigma_r \left\{ r'^2 + r''^2 \right\}^{1/2} / B \qquad (27c)$$

$$\sigma_z = \sigma_r \left\{ r'^2 (y - B)^2 + r''^2 \cdot y^2 \right\}^{1/2} / BH \qquad (27d)$$

An actual stereo-model warp may result from systematic range errors. Cross-track distances and height differences would be affected as follows:

$$d\Delta y_r = \left(\frac{dr' \, y}{B \, r'} - \frac{dr'' \, (y-B)}{B \, r''}\right) \Delta y + \left(\frac{dr' \cdot H}{B \, r'} - \frac{dr'' \cdot H}{B \, r''}\right) \Delta z \qquad (28a)$$

$$d\Delta z_r = \left(\frac{dr' \cdot r'}{B \cdot H} + \frac{dr' \, (y-B) \cdot y}{B \cdot H \cdot r'} - \frac{dr'' \cdot r''}{B \cdot H} - \frac{dr'' \cdot y \cdot (y-B)}{B \cdot H \cdot r''}\right) \Delta y +$$

$$+ \left(\frac{dr' \cdot (y-B)}{B \cdot r'} - \frac{dr' \cdot (y-B) \cdot r}{B \cdot H^2} - \frac{dr'' \cdot y}{B \cdot r''} + \frac{dr'' \cdot y \, r''}{B \cdot H^2}\right) \Delta z \qquad (28b)$$

From these algebraic expressions we can conclude that warping of the stereo model is nonlinear. However, all error coefficients are smaller than 1 so that model height differences and distances can be expected to have errors smaller than those of the source. Again, numerical values are presented in Appendix C.

5.3 DISCUSSION

From the algebraic expressions derived in the previous sections it follows that different results are obtained for errors of *coordinates* versus *distances* or *height-differences*. The formulas and numerical evaluations in Appendix C (Figures C1, C2) show that coordinate errors will be large in both aircraft and spacecraft radar stereo: for aircraft, with comparatively large stereo intersection angles, coordinate errors will be 1 to 5 times larger than the error of sensor position or of range measurement. Heights z will in the near range be more accurate than the across-track coordinate y; at far ranges the situation is reversed; y is more accurate than z.

For satellite radar such as VOIR -- without two distinctly different look angles for overlapping swaths -- the coordinate error will be 8 to 15 times larger than the error of sensor position or of slant range.

In many instances, however, it is not the absolute accuracy that is important, but rather the error of a radargrammetrically measured distance and height difference.

As illustrated in Tables C1, C2 of Appendix C, both across-track distances Δy and height differences Δz are less sensitive to errors of sensor position (stereo base B, sensor height H) or of range r than was found for the coordinates themselves.

In comparing we find, that at the center of an aircraft stereo model such as that shown in Appendix C an error dB of the stereo base B of 100 m will change the observed height of an object point for 261 m, its across-track position for 237 m. Were one to employ VOIR-stereo, then the sensor error dB = 100 m would

result in a height change of 935 m, and a cross-track change of 988 m. A height difference, measured across a horizontal distance Δy would be affected differently in the same area of the stereo model: a base error dB = 100 m would result in an error $d\Delta z$ of the height difference Δz = 1 km (Δy = 1 km) that amounts to -11 m (aircraft) or -2.5 m (VOIR).

The error propagations are similar when considering the effects of other error sources. Systematic errors of slant range have the smallest effect on height differences or distances. However, limited range resolution does not lead to systematic but to random errors. These generate an inaccuracy of measuring height differences and distances that are a factor $\sqrt{2}$ larger then the error of a single coordinate measurement. Thus a range resolution limited to ±100 m for VOIR will create random errors of height differences of $\pm 1.1 \cdot \sqrt{2}$ to $\pm 1.4 \cdot \sqrt{2}$ km, and random errors of cross track distances of $\pm 1.3 \cdot \sqrt{2}$ to $\pm 1.4 \cdot \sqrt{2}$ km.

SECTION 6

CONCLUSION

We have reported basic considerations on stereo side-looking radar, presented a general algorithm for stereo radar intersection and derived algebraic expressions for the errors of point coordinates obtained by stereo-radargrammetry. We have, based on these formulas, given expressions for deformations of stereo models. These deformations concern cross-track distances and height differences and may thus be called "relative accuracies" of coordinate differences. The formulas are presented as derivations and essentially relate to systematic errors of the stereobase, B; of sensor height, H; and of slant ranges, r', r''.

The algebraic expressions were derived using simple geometric considerations. They permit a wealth of conclusions to be drawn on stereo-radar. Some numerical evaluations of the formulas are presented in Appendix C for a general aircraft stereo radar arrangement and for a proposed satellite project VOIR.

Radar stereo can be evaluated using vertical exaggeration as a figure of merit. It was found that the vertical exaggeration is limited for satellite radar stereo if no distinctly different look angles are employed. For VOIR, the vertical exaggeration would not go beyond 0.6, while for aircraft radar optimum visual stereo would produce an exaggeration factor between 1.8 and 2.3. For camera photography, this same factor usually amounts to 3.

Errors of coordinates and of distances measured in the radar stereo-model are systematic when caused by slowly varying errors of the stereo base or of the sensor height. Coordinate errors may be 10 times the size of errors of height differences when using aircraft radar; for VOIR this factor may amount to several hundred: this means that systematic errors of the stereo base, or of the sensor altitude, have a very slowly varying effect on the radar stereo model. Random errors, however, such as those resulting from limited radar resolution, have an effect on distances and height differences that is essentially of the same magnitude as the effect on coordinate errors.

Presently there is only limited knowledge on the optimum radar stereo arrangement: stereo intersection angles should be large from a geometric point of view, but small in order to permit visual stereo perception. Present indications are that visual radar stereo is possible with intersection angles of up to 15°, where angles off nadir should be not smaller than 40°. These are angles that should be used in present planning for future satellite radar missions. Limits to range resolution will considerably magnify the errors of observed height differences and cross-track distances if stereo-intersection angles are chosen that are small. However, in order to understand the exact limits of visual stereo it is necessary that extensive experimental work still be carried out to analyze the interaction of stereo-intersection angles, look angles off nadir, and terrain ruggedness in their effect on the subjective experience of visually measuring and interpreting a radar stereo model.

APPENDIX A

THE IMPOSSIBILITY OF SINGLE FLIGHT STEREO SAR USING NON-ZERO DOPPLER PROCESSING

It will be shown that processing of a single SAR image strip with differential Doppler frequencies does not lead to valid stereo.

A1. THE DOPPLER CONE AND RANGE SPHERE

Imaging with SAR using a non-zero Doppler frequency for correlation is equivalent to imaging with a (synthetic) radar beam of conical shape: from a given sensor position points will be imaged that produce the same Doppler frequency shift -- this implies that they are on the surface of a cone (compare Figure A-1). The locus of an image point for which a slant range r from the sensor has been measured is a sphere, the so-called range sphere (compare Figure A-2).

A2. DESCRIPTIVE GEOMETRIC CONSIDERATIONS CONCERNING RADAR PROJECTION LINES AND STEREO

Given is a point P in a radar image and the sensor's position and attitude when the point was imaged. From the single radar record the geometric locus of the point P can be established as an intersection of the range sphere and Doppler cone.

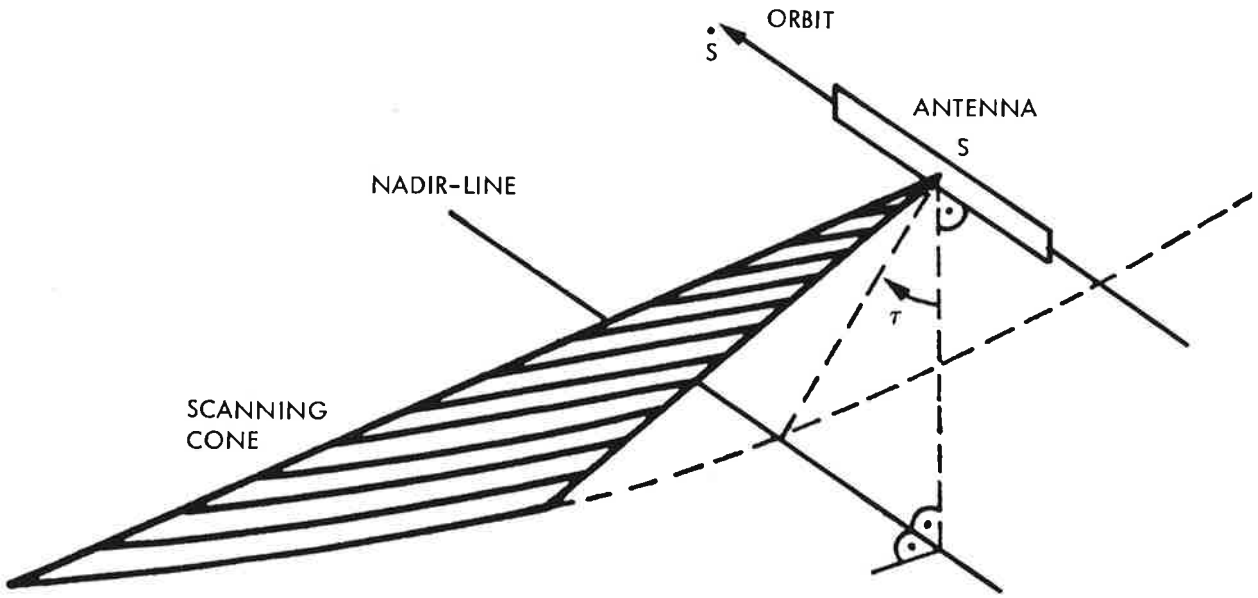

Figure A-1. The Concept of Imaging with "Squint"

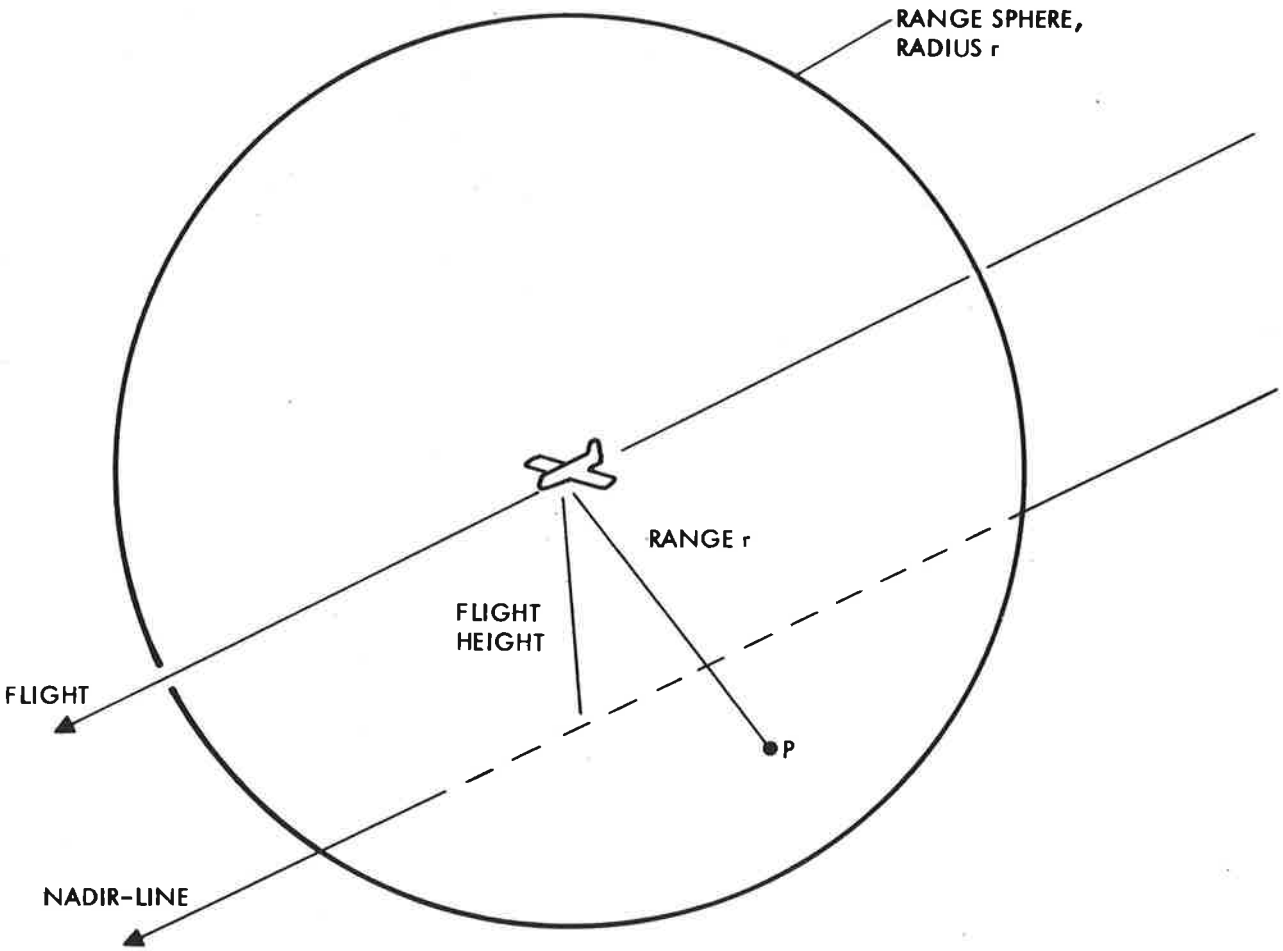

Figure A-2. Range Sphere to Point P

It is trivial to see that the locus of point P is a circle concentric with respect to the flight line and in a plane perpendicular to it (compare Figure A-3).

From this we can conclude that radar projection lines are circles. This fact was illustrated by Figure 9 in the main part of the report.

If we assume a reference datum for the imaged surface, then we can define a "*ground range presentation*" according to Figure 9. Points outside this reference will show *relief-displacement* according to Figure 10. Radar stereo is based on different relief displacements in overlapping stereo image pairs, for example as shown in Figure 12 for stereo with two flight lines. It is obvious that no stereo is obtained with images that display identical relief displacements.

From the above we can conclude that for a given single flight line one will obtain for any given object point exactly the same projection circle, whatever the Doppler cone angle τ may be: two correlations with different Doppler frequencies (positive and negative, for example) will result in the same projection circle. An intersection is not defined (compare Figure A-4).

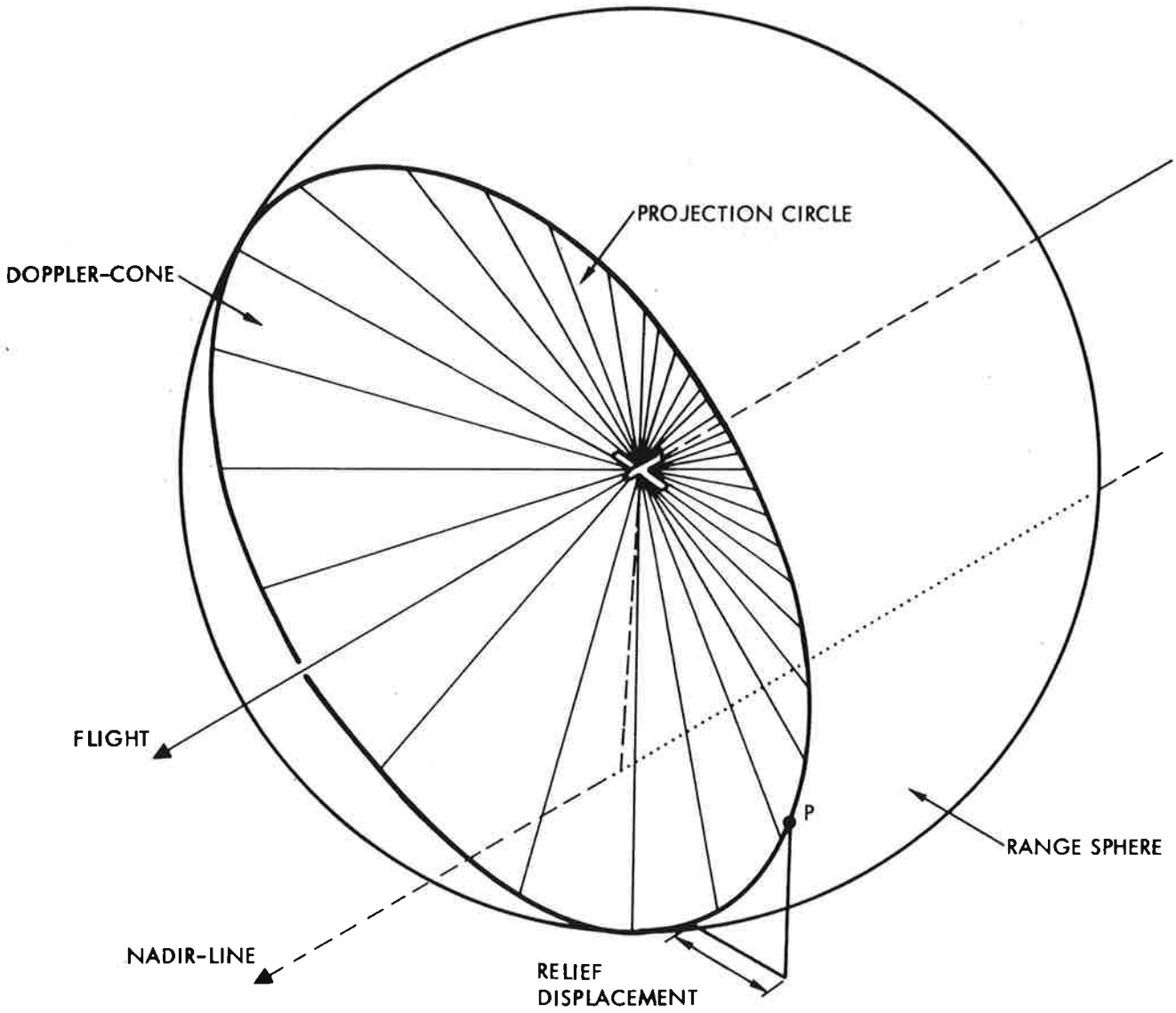

Figure A-3. Definition of the Intersection of Range Sphere and Doppler Cone. Result is a "projection line" for an object point P.

In other words: relief displacement will always be the same irrespective of Doppler frequency. Mountains will always fall towards the nadir line in a direction perpendicular to that line. Therefore two images will not produce the desired stereo model of the object.

However, one may obtain the visual impression of an overall bow of the imaged area, if two differential correlations are viewed under a stereoscope. This may be due to an overall deformation of systematic nature, depending on how the correlations are being produced. That, however, is not a stereo model of the terrain relief.

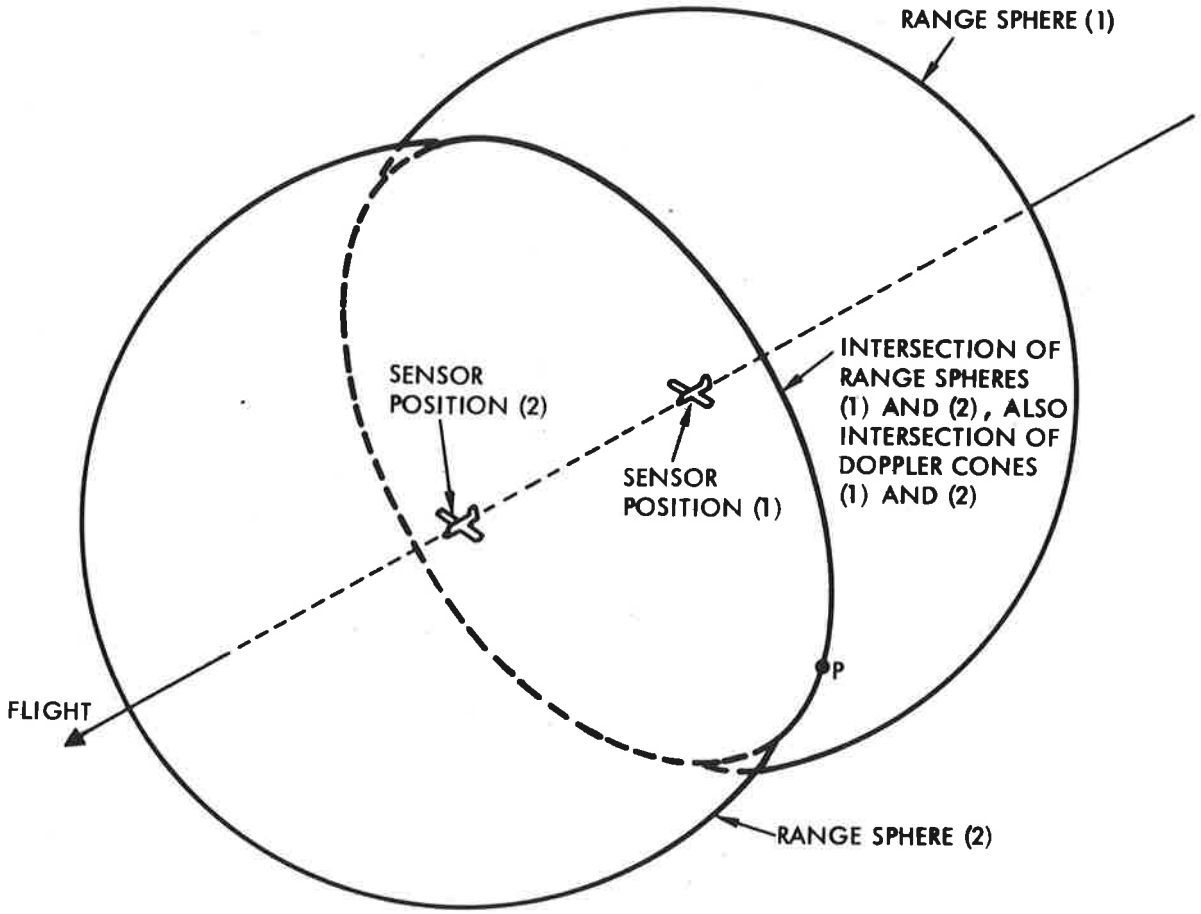

Figure A-4. Intersection of Two Projection Lines in Single Flight "Stereo" Arrangement with Non-Zero Doppler Processing not Defined. Intersection Lines of Range Sphere and Doppler Cone Coincide.

A3. ALGEBRAIC CONSIDERATIONS

The facts of Section A2 will now be discussed algebraically. For clarity some assumptions are made about the coordinate systems.

A coordinate system is defined with axes x, y, z, where x is parallel to the flight path. The sensor moves along a straight line in the xz coordinate plane (compare Figure A-5).

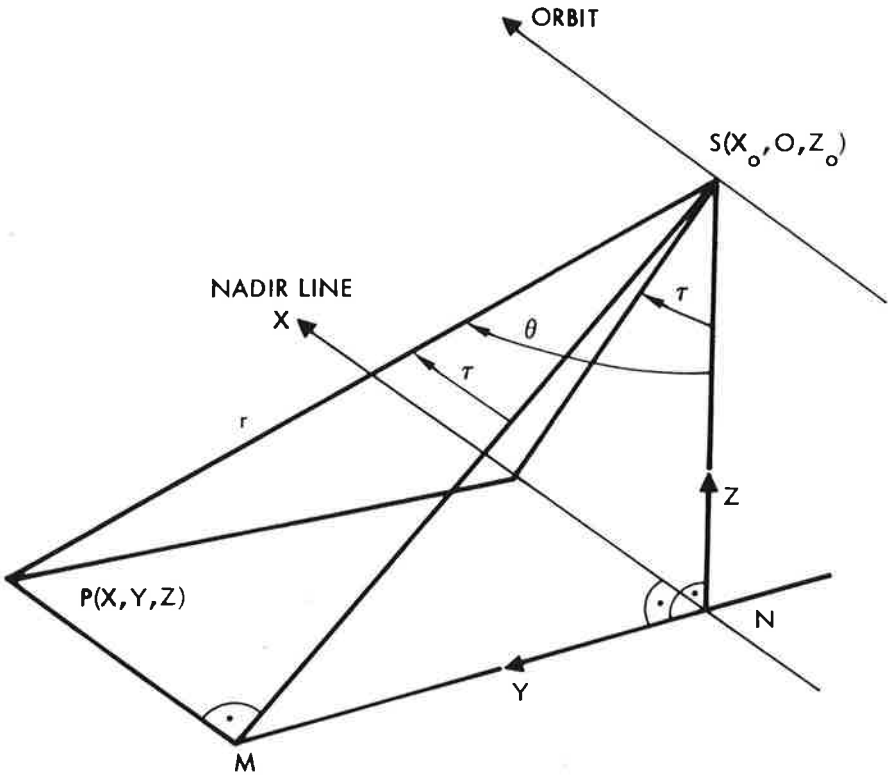

Figure A-5. Definitions for the Formulation of Equations (A1) to (A6)

We define the position of the sensor by the vector $\underline{s}' = (x_o', 0, z_o)$, the position of the object point P by the vector $\underline{p} = (x, y, z)$. The cone angle is designated by τ'.

We find the equation of the range sphere as:

$$(x - x_o')^2 + y^2 + (z - z_o)^2 = r'^2 \qquad \text{(A1)}$$

We find the equation of the Doppler cone as:

$$(x - x_o') / \sin \tau' = r' \qquad \text{(A2)}$$

The intersection of range sphere (A1) and cone (A2) is found by substitution of (2) into (1):

$$y^2 + (z - z_o)^2 = r'^2 - r'^2 \sin^2 \tau'$$

and

$$y^2 + (z - z_o)^2 = r'^2 \cos^2 \tau' \qquad \text{(A3)}$$

This is a circle in a plane x = constant. The center of the circle is at $(x, 0, z_o)$, its radius is $r' \cos \tau'$

Equation (A3) represents the projection line obtained from sensor position $\underline{s}'$ using a cone angle τ'.

A second correlation with a different cone angle τ'', but from the same object $\underline{p} = (x, y, z)$ corresponds to a sensor position $\underline{s}'' = (x_o'', 0, z_o)$, where x_o'' results from Equation (A2):

$$(x - x_o'') / \sin \tau'' = r'' \qquad \text{(A4)}$$

The projection circle is given by:

$$y^2 + (z - z_o)^2 = r''^2 \cos^2 \tau'' \qquad \text{(A5)}$$

The second projection circle is also in the plane x = constant, with the center at $(x, 0, z_o)$. Since it has to pass through the point $\underline{p}$ we obtain the identity:

$$r'^2 \cos^2 \tau' = r''^2 \cos^2 \tau'' \qquad \text{(A6)}$$

This identity confirms that both images produce the same projection circle, so that there is no intersection defined. We must conclude that no valid stereo is possible.

A4. CONCLUSIONS

This appendix proves that single flight stereo with SAR is not possible on the basis of two correlations using different Doppler frequencies.

A strictly rectilinear flight line was assumed. However, conclusions remain unaltered with small deviations of the flights from a straight line.

APPENDIX B

STRICT SOLUTION TO THE RADAR STEREO INTERSECTION PROBLEM

B.1 ALGORITHM

The stereo radargrammetric computation may start out from Equations (6) of Section 3. If we assume that we deal with SAR and that image presentation is without the effect of squint angle τ ($\tau = o$), we obtain for each point:

$$\begin{aligned} |\underline{p} - \underline{s}'| &= r' \\ |\underline{p} - \underline{s}''| &= r'' \\ \dot{\underline{s}}' \cdot (\underline{p} - \underline{s}') &= 0 \\ \dot{\underline{s}}'' \cdot (\underline{p} - \underline{s}'') &= 0 \end{aligned} \qquad \text{(B.1)}$$

with

$$\underline{p} = (x, y, z)^T$$

$$\underline{s} = (x_o, y_o, z_o)^T$$

$$\dot{\underline{s}} = (\dot{x}_o, \dot{y}_o, \dot{z}_o)^T$$

This is a nonlinear system of equations for the unknown coordinates $\underline{p} = (x, y, z)^T$. For a least squares algorithm we need to linearize:

$$C \cdot \underline{v} + \underline{D}\,\Delta\underline{p} + \underline{f} = 0 \qquad \text{(B.2)}$$

where $\Delta\underline{p}$ is the vector of corrections to the approximate solution $\tilde{\underline{p}}$, $\underline{v}$ is the vector of observational errors, $\underline{f}$ is the vector of contradictions. We find:

$$\Delta\underline{p} = (\Delta x, \Delta y, \Delta z)^T$$

$$\underline{v} = v_{xo}', v_{yo}', v_{zo}', v_{\dot{x}o}', v_{\dot{y}o}', v_{\dot{z}o}', v_r', v_{xo}'', v_{yo}'',$$

$$v_{zo}'', v_{\dot{x}o}'', v_{\dot{y}o}'', v_{\dot{z}o}'', v_r'')^T$$

so that an improved approximation $\tilde{\tilde{\underline{p}}}$ of $\tilde{\underline{p}}$ is found:

$$\tilde{\tilde{\underline{p}}} = \tilde{\underline{p}} + \Delta\underline{p} \qquad \text{(B.3)}$$

Matrix $\underline{C}$ is:

$$\begin{aligned}
C_{1,1} &= -2\,(x - x_o') \\
C_{1,2} &= -2\,(y - y_o') \\
C_{1,3} &= -2\,(z - z_o') \\
C_{1,7} &= -2\,r' \\
C_{2,8} &= -2\,(x - x_o'') \\
C_{2,9} &= -2\,(y - y_o'') \\
C_{2,10} &= -2\,(z - z_o'') \\
C_{2,14} &= -2\,r'' \\
C_{3,1} &= -\dot{x}_o' \\
C_{3,2} &= -\dot{y}_o' \\
C_{3,3} &= -\dot{z}_o' \\
C_{3,4} &= (x - x_o') \\
C_{3,5} &= (y - y_o') \\
C_{3,6} &= (z - z_o') \\
C_{4,8} &= -\dot{x}_o'' \\
C_{4,9} &= -\dot{y}_o'' \\
C_{4,10} &= -\dot{z}_o'' \\
C_{4,11} &= (x - y_o'') \\
C_{4,12} &= (y - y_o'') \\
C_{4,13} &= (z - z_o'')
\end{aligned}$$

All other elements of $\underline{C}$ are zero. For $\underline{D}$:

$$
\begin{aligned}
D_{1,1} &= 2\,(x - x_o') \\
D_{1,2} &= 2\,(y - y_o') \\
D_{1,3} &= 2\,(z - z_o') \\
D_{2,1} &= 2\,(x - x_o'') \\
D_{2,2} &= 2\,(y - y_o'') \\
D_{2,3} &= 2\,(z - z_o'') \\
D_{3,1} &= \dot{x}_o' \\
D_{3,2} &= \dot{y}_o' \\
D_{3,3} &= \dot{z}_o' \\
D_{4,1} &= \dot{x}_o'' \\
D_{4,2} &= \dot{y}_o'' \\
D_{4,3} &= \dot{z}_o''
\end{aligned}
$$

For $\underline{f}$:

$$f_1 = -\,|\tilde{\underline{p}} - \underline{s}'| - r'$$

$$f_2 = -\,|\tilde{\underline{p}} - \underline{s}''| - r''$$

$$f_3 = -\dot{\underline{s}}' \cdot (\tilde{\underline{p}} - \underline{s}')$$

$$f_4 = -\dot{\underline{s}}'' \cdot (\tilde{\underline{p}} - \underline{s}'')$$

The least squares method leads then to:

$$\Delta\underline{p} = -\,(\underline{D}^T\,(\underline{C}\;\underline{Q}\;\underline{C}^T)^{-1}\;\underline{D})^{-1}\;D^T\;(\underline{C}\;\underline{Q}\;\underline{C}^T)^{-1}\;\underline{f} \qquad \text{(B.4)}$$

where $\underline{Q}$ is the variance-covariance matrix of the observed quantities x_o', y_o', z_o', $\dot{x}_o'$, $\dot{y}_o'$, $\dot{z}_o'$, r', x_o'', y_o'', z_o'', $\dot{x}_o''$, $\dot{y}_o''$, $\dot{z}_o''$, r'' and must be available a priori.

The algorithm is iterative. After a preliminary computation to find an approximate solution $\tilde{\underline{p}}$, one computes $\underline{C}$, $\underline{D}$, $\underline{f}$ and $\Delta\underline{p}$. With an improved $\tilde{\tilde{\underline{p}}} = \tilde{\underline{p}} + \Delta\underline{p}$ one repeats the procedure until $\Delta\underline{p}$ becomes insignificantly small.

B.2 COMMENTS

The above algorithm is simple and straightforward. In the event that not SAR, but real aperture is available, one must substitute for $\dot{\underline{s}}$ the vector in the direction of the physical antenna. This direction can be described by pitch ϕ and yaw angle κ:

$$\begin{aligned} x_o &= \cos\phi \cos\kappa \\ y_o &= \cos\phi \sin\kappa \\ z_o &= -\sin\phi \end{aligned} \qquad \text{(B.5)}$$

A totally different stereo computation results if Equation (5) of Section 3 is used as follows:

$$\underline{s}' + \underline{r}' - \underline{s}'' - \underline{r}'' = 0 \qquad \text{(B.6)}$$

This is a coplanarity condition for the two orbit stations ($'$), ($''$) and the unknown point. It consists of three equations with two unknowns Ω', Ω'' since:

$$\underline{r}' = \underline{A}\,\underline{r}_o' \qquad \text{(B.7)}$$

where

$$\underline{r}_o' = (\sin\tau,\ (\sin^2\Omega' - \sin^2\tau)^{1/2},\ \cos\Omega') \qquad \text{(B.8)}$$

$\underline{A}$ ..... rotation matrix

Vector $\underline{r}_o'$ gives the point in the antenna coordinate system, while $\underline{A}$ rotates that system into the reference coordinate system.

Details about the stereo computation with Equation (B.6) can be found in the literature (Leberl, 1976 a, 1976 b, 1978) together with a numerical comparison of the two alternatives. The approach with Equation (B.1) appeared to be somewhat superior in an application to lunar Apollo 17 - ALSE - VHF imagery with small stereo intersection angles of 3°.

APPENDIX C

DEFORMATIONS OF RADAR STEREO MODELS

Equations (18), (19), (22), and (24), (26), (28) have been evaluated for two stereo arrangements as shown in Figure C-1. For the aircraft radar, the angles of stereo intersection are $26^\circ > \Delta\theta > 8.6$, with $52.4 < \theta' < 68.2$ and $26.6 < \theta'' < 59.5$. For VOIR, $3.3 > \Delta\theta > 2.8$, $44.2 < \theta' < 48.6$, $40.9 < \theta'' < 45$. Overlap of images is 60%.

Presented are error coefficients, not errors themselves. Figure C-2 shows aircraft stereo model coordinate errors dy, dz due to dy_o'', dz_o'', dr', whereby the y-coordinate is plotted on the abscissa. For the example of dy_o'', a model error dy will be produced in the near range that is twice to 3 times the amount of dy_o''. It is obvious that the height error dz varies more than dy with increasing range, and that it is particularly affected at far ranges by dy_o'', dr'.

Tables C-1, C-2 present the errors of height differences Δz and distances Δy, again in the form of coefficients: for the example of a base error dB in VOIR, the height difference Δz = 3 km, measured across a Δy of 1 km at near range (y = 365 km) will have an error $d\Delta z$ of 0.017 · dB.

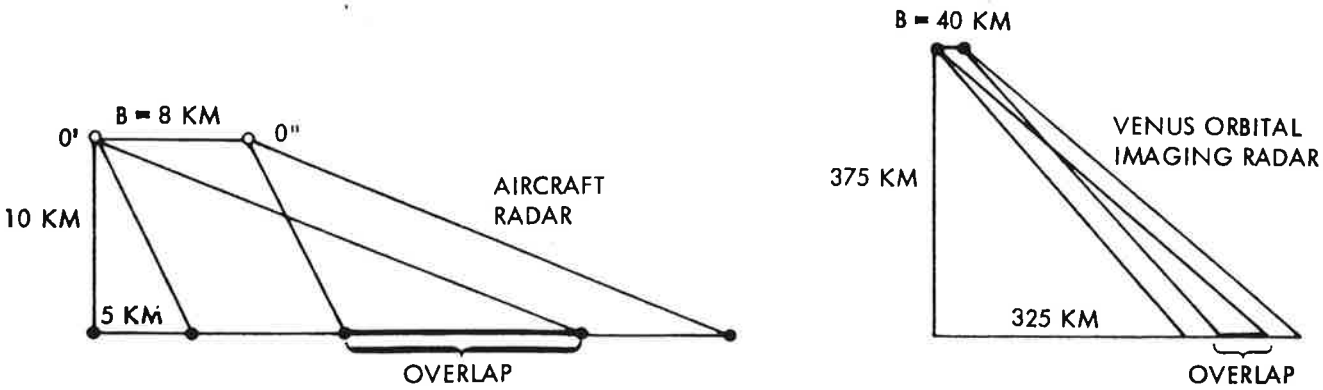

Figure C-1. Stereo Arrangements for Numerical Analysis

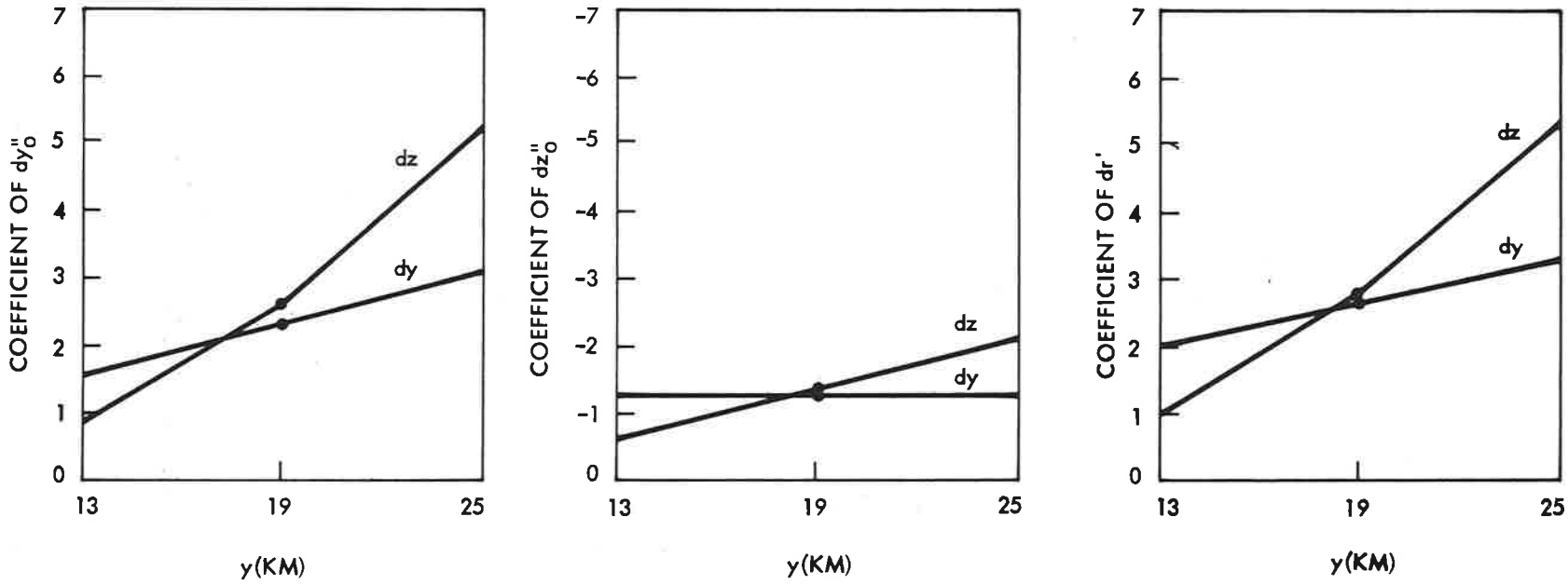

Figure C-2. Coefficients of Sensor Position Errors dy_o'', dz_o'' and of Range Error dr' in the Equation for the Resulting Coordinate Errors dy, dz in the Stereo Model from Aircraft Radar, Figure C-1.

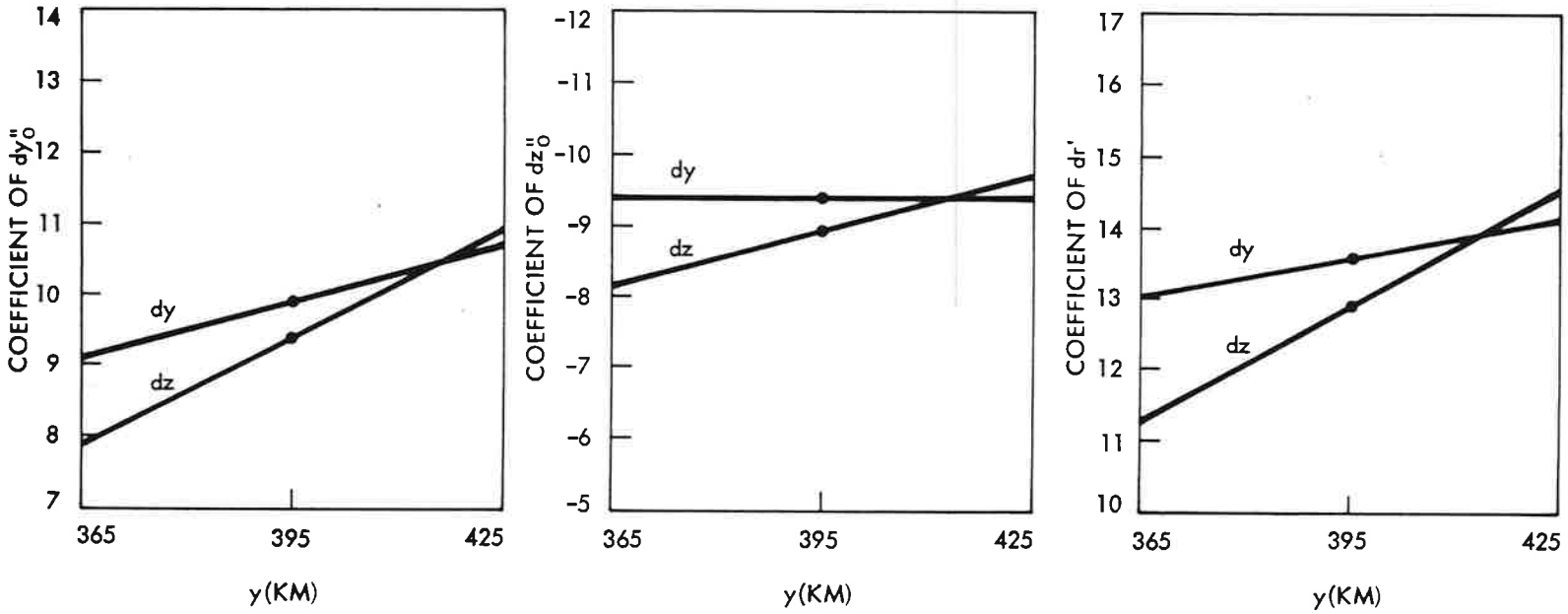

Figure C-3. Coefficients of Sensor Position Errors dy_o'', dz_o'' and of Range Error dr' in the Equation for the Resulting Coordinate Errors dy, dz in the Stereo Model from VOIR, Figure C-1.

Table C-1. Coefficients of Errors dB, dH, dr in the Equations for the Errors dΔz of Height Differences Δz, and for Errors dΔy of Distances Δy, in an Aircraft Stereo Model of Figure C-1.

Error Coefficients								
Base dB		Height dH		Range dr		(km)		
Δy	Δz	Δy	Δz	Δy	Δz	Δz	Δy	y
0.000	0.000	0.000	0.000	0.000	0.000	0		
0.000	0.081	0.125	0.000	-0.036	-0.028	1	0	
0.000	0.244	0.375	0.000	-0.107	-0.084	3		
-0.125	-0.225	0.000	0.125	0.043	0.042	0		
-0.125	-0.144	0.125	0.125	0.008	0.014	1	1	13
-0.125	0.019	0.375	0.125	-0.064	-0.042	3		
-0.625	-1.125	0.000	0.625	0.216	0.211	0		
-0.625	-1.044	0.125	0.625	0.180	0.183	1	5	
-0.625	-0.881	0.375	0.625	0.109	0.126	3		
0.000	0.000	0.000	0.000	0.000	0.000	0		
0.000	0.261	0.125	0.000	-0.026	-0.038	1	0	
0.000	0.784	0.375	0.000	-0.078	-0.114	3		
-0.125	-0.375	0.000	0.125	0.018	0.029	0		
-0.125	-0.114	0.125	0.125	-0.008	-0.009	1	1	19
-0.125	0.409	0.375	0.125	-0.059	-0.085	3		
-0.625	-1.875	0.000	0.625	0.091	0.143	0		
-0.625	-1.614	0.125	0.625	0.065	0.105	1	5	
-0.625	-1.091	0.375	0.625	0.013	0.029	3		
0.000	0.000	0.000	0.000	0.000	0.000	0		
0.000	0.531	0.125	0.000	-0.017	-0.035	1	0	
0.000	1.594	0.375	0.000	-0.051	-0.106	3		
-0.125	-0.525	0.000	0.125	0.008	0.018	0		
-0.125	0.006	0.125	0.125	-0.009	-0.017	1	1	25
-0.125	1.069	0.375	0.125	-0.043	-0.088	3		
-0.625	-2.625	0.000	0.625	0.042	0.090	0		
-0.625	-2.094	0.125	0.625	0.025	0.055	1	5	
-0.625	-1.031	0.375	0.625	-0.009	-0.016	3		

Table C-2. Coefficients of Errors dB, dH, dr in the Equations for the Errors dΔz of Height Differences Δz, and for Errors dΔy of Distances Δy in a VOIR Stereo Arrangement of Figure C-1.

Error Coefficients								
Base dB		Height dH		Range dr				
Δy	Δz	Δy	Δz	Δy	Δz	Δz	Δy	y
0.000	0.000	0.000	0.000	0.000	0.000	0		
0.000	0.021	0.025	0.000	-0.001	-0.001	1	0	
0.000	0.063	0.075	0.000	-0.003	-0.003	3		
-0.025	-0.046	0.000	0.025	0.001	0.001	0		
-0.025	-0.025	0.025	0.025	0.000	0.000	1	1	365
-0.025	0.017	0.075	0.025	-0.002	-0.002	3		
-0.125	-0.230	0.000	0.125	0.005	0.005	0		
-0.125	-0.209	0.025	0.125	0.004	0.004	1	5	
-0.125	-0.167	0.075	0.125	0.002	0.002	3		
0.000	0.000	0.000	0.000	0.000	0.000	0		
0.000	0.025	0.025	0.000	-0.001	-0.001	1	0	
0.000	0.075	0.075	0.000	-0.003	-0.003	3		
-0.025	-0.050	0.000	0.025	0.001	0.001	0		
-0.025	-0.025	0.025	0.025	0.000	0.000	1	1	395
-0.025	0.025	0.075	0.025	-0.002	-0.002	3		
-0.125	-0.250	0.000	0.125	0.005	0.005	0		
-0.125	-0.225	0.025	0.125	0.004	0.004	1	5	
-0.125	-0.175	0.075	0.125	0.002	0.002	3		
0.000	0.000	0.000	0.000	0.000	0.000	0		
0.000	0.029	0.025	0.000	-0.001	-0.001	1	0	
0.000	0.087	0.075	0.000	-0.003	-0.003	3		
-0.025	-0.054	0.000	0.025	0.001	0.001	0		
-0.025	-0.025	0.025	0.025	-0.000	-0.000	1	1	425
-0.025	0.033	0.075	0.025	-0.002	-0.002	3		
-0.125	-0.270	0.000	0.125	0.004	0.005	0	5	
-0.125	-0.241	0.025	0.125	0.003	0.004	1		
-0.125	-0.183	0.075	0.125	0.001	0.002	3		

REFERENCES

1. Aschenbrenner, C.M. (1952): "A Review of Facts and Terms Concerning the Stereoscopic Effect", Photogrammetric Eng., Vol. 18.

2. Bair, A.L., G.E. Carlson (1974): "Performance Comparison of Techniques for Obtaining Stereo Radar Images", IEEE Trans. on Geoscience Electronics, GE-11.

3. Bair, G.L., G.E. Carlson (1975): "Height Measurement with Stereo Radar", Photogrammetric Eng. and Remote Sensing, Vol. XLI.

4. Carlson, G.E. (1973): "An Improved Single Flight Technique for Radar Stereo", IEEE Trans. on Geoscience Electronics, GE-11, No. 4.

5. Clerici, E., G. Konecny (1978): "A Study in the Determination of Depth Information from Underwater Acoustical Scanners," Symposium of Comm. III, Int. Soc. of Photogrammetry, Moscow, USSR, 31 July - 5 August 1978. Published in: Nachrichten aus dem Karten-und Vermessungswasen, Reike II, 36, Inst. for Applied Geodesy, Frankfurt a.M., Germany.

6. Dalke, G., M. McCoy (1968): "Regional Slopes with Non-Stereo Radar," Photogrammetric Engineering, Vol. 34.

7. DBA-Systems (1974): "Research Studies and Investigations for Radar Control Extensions", DBA Systems, Inc., P.O. Drawer 550, Melbourne, Florida, Defense Documentation Center Report No. 530784L.

8. Derenyi, E.E. (1975): "Topographic Accuracy of Side Looking Radar Imagery", Bildmessung und Luftbildwesen, 1975, No. 1.

9. Fichter, A.J. (1954): "Geometry of the Imaginary Stereo Model", Photogrammetria, Vol. 10, pp. 134-139.

10. Goodyear (1974): "Preliminary Imagery Data Analysis Goodyear Electronic Mapping System (GEMS)", Goodyear Aerospace Corp., Report GIB-9342, Code 99696.

11. Graham, L. (1975): "Flight Planning for Stereo Radar Mapping", Proc. Am. Soc. Photogramm., 41st Meeting, Washington, D.C.

12. Graham, L. (1976): "Earth Resources Radar Stereo Considerations", Goodyear Aerospace Corp., Arizona Div., AEEM-550, 13 p.

13. Gracie, G. et al (1970): "Stereo Radar Analysis", U.S. Engineer. Topographic Laboratory, Ft. Belvoir, Virginia. Report No. FTR-1339-1.

14. Innes, R.B. (1964): "Principles of SLAR Measurement of the Third Coordinate of Target Position", Report of Project Michigan No. 2900-474-T.

15. Konecny, G. (1972): "Geometrical Aspects of Remote Sensing", Arch. Int. Soc. Photogramm., Invited Paper, 12th Congress, Ottawa, Canada.

16. Koopmans, B. (1974): "Drainage Analysis on Radar Images", ITC-Journal, 1973-3, Enschede, Netherlands.

17. Laprade, G. (1963): "An Analytical and Experimental Study of Stereo for Radar", Photogrammetric Engineering, Vol. 29.

18. LaPrade, G.L. (1970): "Subjective Considerations for Stereo Radar", Goodyear Aerospace Corp., GiB 9169.

19. LaPrade, G. (1972): "Stereoscopy - A More General Theory", Photogrammetric Engineering, Vol. 38, pp. 1177 - 1187.

20. LaPrade, G. (1973a): "Stereoscopy - Will Facts or Dogma Prevail?", Photogrammetric Engineering, Vol. 39, pp. 1271 - 1275.

21. LaPrade, G. (1973b): "A More General Theory of Stereoscopy", Goodyear Aerospace Corp., Arizona Div., GiB-9268, Rev. A, 58 p.

22. LaPrade, G. (1975): Addendum to GiB-9169, "Subjective Considerations for Stereo Radar", Goodyear Aerospace Corp., Arizona Division.

23. LaPrade, G. et al (1975): "Stereoscopy", Goodyear Aerospace Corp., Arizona Div., GERA-2120, Code 99696; 57 p.

24. Leberl, F. (1972): "On Model Formation with Remote Sensing Imagery," Österr, Zeitschrift für Vermessungswasen, Vol. 60, pp. 93-61.

25. Leberl, F. (1975): "Radargrammetry for Image Interpreters", ITC Techn. Report No. 2, Enschede.

26. Leberl, F. (1976a): "Mapping of Lunar Surface from Side-Looking Orbital Radar Images", The Moon, Vol. 15, No. 3/4.

27. Leberl, F. (1976b): "Imaging Radar Applications to Mapping and Charting", Photogrammetria, Vol. 32.

28. Leberl, F. (1978): "Satellitenradargrammetrie", Deutsche Geodatische Kommission, Series C, Nr. 239, Munich, 156 p.

29. Nowicki, A.L. (1966): "Stereoscopy", Chapter 11 of Manual of Photogrammetry, 3rd edition, American Soc. of Photogrammetry, Falls Church, Va., USA.

30. Rosenfield, G.H. (1968): Stereo Radar Techniques, Photogrammetric Engineering, Vol. 34.

NASA—JPL—Coml., L.A., Calif.